12

PHYSICAL AND MAGNETIC PROPERTIES

12.0   INTRODUCTION

In this last chapter we cover techniques for measuring surface areas, surface roughness, and surface and thin-film magnetism. In addition, the effects that sputter-induced surface roughness has on depth profiling methods are discussed.

Six methods for determining roughness are briefly explained and compared. They are mechanical profiling using a stylus; optical profiling by interferometry of reflected light with light from a flat reference surface; the use of SEM, AFM, and STM (see Chapter 2), and, finally, optical scatterometry, where light from a laser is reflected from a surface and the amount scattered out of the specular beam is measured as a function of scattering angle. All except optical scatterometry are scanning probe methods. A separate article is devoted to optical scatterometry. The different methods have their own strengths and weaknesses. Mechanical profiling is cheap and fast, but a tip is dragged in contact across the surface. The roughness "wavelength" has to be long compared to the stylus tip radius (typically 3 μm) and the amplitude small for the tip to follow the profile correctly. Depth resolution is about 5 Å. The optical profiler is a noncontact method, which can give a three-dimensional map, instead of a line scan, with a depth resolution of 1 Å. It cannot handle materials that are too rough (amplitudes larger than 1.5 μm) and if the surface is not completely reflective, reflection from the interior regions, or back interfaces, can

cause problems. The lateral resolution depends on the light wavelength used, but is typically around 0.5 μm. The SEM operates in vacuum and requires a conducting surface, but is capable of 10-Å resolution in both vertical and lateral directions. AFM/STM measurements can provide surface topology maps with depth resolution down to a fraction of an angstrom and lateral resolution down to atomic dimensions. For practical surfaces, however, the instruments are usually operated in air at lower resolution. Optical Scatterometry is rather different in concept from the other methods in that it gives statistical information on the range of roughness, for flat reflective surfaces, within the area struck by the laser beam. Root-mean-squared (RMS) roughness values can be extracted from the data with a depth resolution of 1 Å. It can also be used to characterize the shapes and dimensions of periodic structures on a flat surface (e.g., patterned silicon wafers) with dimensions in the sub-μm range. To do this requires, however, calculation of the scattering behavior from an assumed model and a fit to the data. Optical scatterometry has been successfully used during on-line processing.

For many of the techniques discussed in this volume, composition depth profiling into a solid material is achieved by taking a measurement that is surface sensitive while sputtering away the material. Unfortunately, sputtering does not remove material uniformly layer by layer but introduces topography that depends on the material, the angle of sputtering, and the energy of the sputtering. This always degrades the depth resolution of the analysis technique with increasing depth. Specific examples are described here, as well as ways that the effect can be minimized.

In Magneto-Optic Kerr Rotation, MOKE, the rotation in polarization occurring when polarized laser light reflects from a magnetized material is measured. The rotation is due to the interaction of the light with the unpaired, oriented, valence electron spins of the magnetized sample. The degree of rotation is directly proportional to the magnetic moment, M, of the material, though absolute values of M are hard to obtain this way. This is because of the complex mathematical relationships between rotation and M, and the many artifacts that can occur in the experimental arrangement and also contribute to rotation. Usually, therefore, the method is used qualitatively to follow magnetic changes. These are either hysteresis loops in applied fields, or the use of a dynamic imaging mode to observe the movements and switching of magnetic domains in magnetic recording material. The lateral resolution capability is wavelength dependent and is about 0.5 μm for visible light. Sensitivity is enough to dynamically map domains at up to MHz switching frequencies. The depth of material probed depends on the light penetration depth; about 20–40 nm for magnetic material. Absolute sensitivity is high enough, though, to study monolayer amounts of magnetic material on a nonmagnetic substrate. Magnetic material buried under transparent overlayers can obviously be studied and this configuration is, in fact, the basis of magneto-optic data storage, which uses Kerr rotation to detect the magnetic bits. The technique is nondestructive and can be performed in ambient environments.

The final article of the volume deals with the use of adsorption isotherms to determine surface area. The amount of gas adsorbed at a surface can be determined volumetrically, or occasionally gravimetrically, as a function of applied gas pressure. Total surface areas are determined by physisorbing an inert gas (N_2 or Ar) at low temperature (77 K), measuring the adsorption isotherm (amount adsorbed versus pressure), and determining the monolayer volume (and hence number of molecules) from the Brunauer–Emmett–Teller equation. This value is then converted to an area by multiplying by the (known) area of a physisorbed molecule. The method is widely applied, particularly in the catalysis area, but requires a high surface area of material (at least 1 m^2/gm): e.g., powders, porous materials, and large-area films. Selective surface areas of one material in the presence of another (e.g., metal particles on an oxide support) can sometimes be measured in a similar manner, but by using chemisorption where a strong chemical bond is formed between the adsorbed species and the substrate material of interest. Hydrogen is most commonly used for this, since by now it is known that for many metals it dissociates and forms one adsorbed H-atom per surface metal atom. From the measurement of the amount of hydrogen adsorbed and a knowledge of the spacing between metal atoms (i.e., a knowledge of the crystallographic surfaces exposed) the metal surface area can be determined.

12.1 Surface Roughness

Measurement, Formation by Sputtering, Impact on Depth Profiling

FRED A. STEVIE

Contents

- Introduction
- Measurement Techniques
- Roughness Formed by Sputtering
- Impact on Depth Profiling

Introduction

A surface property that has a direct impact on the results of many types of analysis is its texture or roughness. Roughness can also affect friction and other mechanical properties. A high percentage of surface analytical effort has been expended on samples that have very flat surfaces, such as polished silicon wafers, but there are many other materials of interest, for example, metals and ceramics, that can have roughness on the order of micrometers. Even a polished silicon surface has topographical variations that can be measured by very sensitive techniques, such as atomic force microscopy or scanning tunneling microscopy.

Two surface roughness terms are commonly used: average roughness RA and root-mean-square roughness RMS. For N measurements of height z and average height $\bar{z}$, the average roughness is the mean deviation of the height measurements

$$RA = \frac{1}{N} \sum_{i=1}^{N} \left| z_i - \bar{z} \right| \tag{1}$$

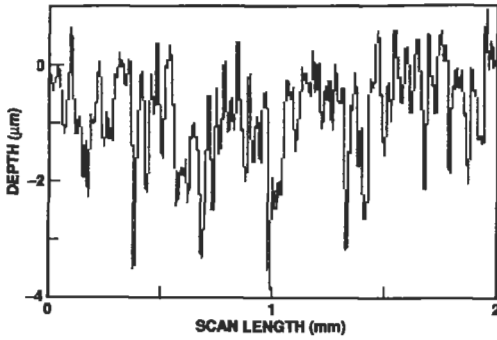and the root-mean-square roughness is the standard deviation

Figure 1   Mechanical profiler trace of a region on the unpolished back of a silicon wafer.

$$RMS = \left[\frac{1}{N} \sum_{i=1}^{N} (z_i - \bar{z})^2 \right]^{1/2} \tag{2}$$

Several surface roughness measurement techniques are in common usage. The optimum method will depend upon the type and scale of roughness to be measured for a particular application.

Measurement Techniques

Mechanical Profiler

Mechanical profilers, also called profilometers, measure roughness by the mechanical movement of a diamond stylus over the sample of interest. No sample preparation is required and almost any sample that will not be deformed by the stylus can be measured very rapidly. The trace of the surface is typically digitized and stored in a computer for display on a cathode ray tube and for output to a printer. The stylus force can be adjusted to protect delicate surfaces from damage. Typical weight loading ranges from a few milligrams to tens of milligrams, but can be as low as one milligram. Small regions can be located with a microscope or camera mounted on the profiler. Lateral resolution depends upon the stylus radius. If the surface curvature exceeds the radius of curvature of the stylus, then the measurement will not provide a satisfactory reproduction of the surface. A typical stylus radius is about 3 μm, but smaller radii down to even submicron sizes are available. Arithmetic average or root-mean-square roughness can be calculated automatically from the stored array of measurement points.

As an example, consider the unpolished back of a silicon wafer. Figure 1 shows a mechanical profiler trace of a region on the wafer. The surface has variations that are generally 1–2 μm, but some of the largest changes in height exceed 3 μm. The average roughness is 0.66 μm.
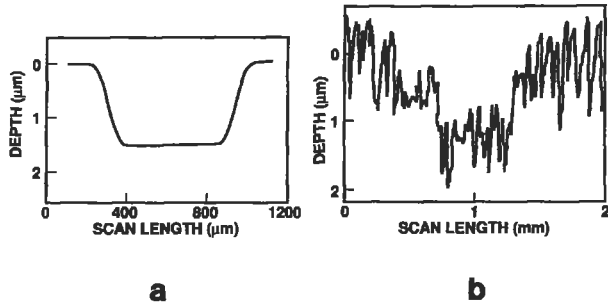
Figure 2 Mechanical profiler traces of craters sputtered with O_2^+ primary beam for an initially smooth surface of Si_3N_4/Si (a); and an initially rough SiC surface (b).

Mechanical profilers are the most common measurement tool for determining the depth of craters formed by rastered sputtering for analysis in techniques like Auger Electron Spectroscopy (AES) and Secondary Ion Mass Spectrometry (SIMS). Figure 2a shows an example of a 1.5-μm deep crater formed by a rastered oxygen beam used to bombard an initially smooth silicon nitride surface at 60° from normal incidence. The bottom of the crater has retained the smooth surface even though the 0.45-μm nitride layer has been penetrated. Depth resolution for an analytical measurement at the bottom of the crater should be good. Figure 2b shows a crater approximately 1 μm deep formed under similar conditions, but on a surface of silicon carbide that was initially rough. The bottom of the crater indicates that the roughness has not been removed by sputtering and that the depth resolution for a depth profile in this sample would be poor.

Even though the mechanical profiler provides somewhat limited two dimensional information, no sample preparation is necessary, and results can be obtained in seconds. Also, no restriction is imposed by the need to measure craters through several layers of different composition or material type.

Optical Profiler

Optical interferometry can be used to measure surface features without contact. Light reflected from the surface of interest interferes with light from an optically flat reference surface. Deviations in the fringe pattern produced by the interference are related to differences in surface height. The interferometer can be moved to quantify the deviations. Lateral resolution is determined by the resolution of the magnification optics. If an imaging array is used, three-dimensional (3D) information can be provided.

Figure 3 shows an optical profiler trace of the same portion of the wafer sample analyzed by the mechanical profiler. The resulting line scan in Figure 3a is similar to that for the mechanical system. The average and root-mean-square roughness are

A

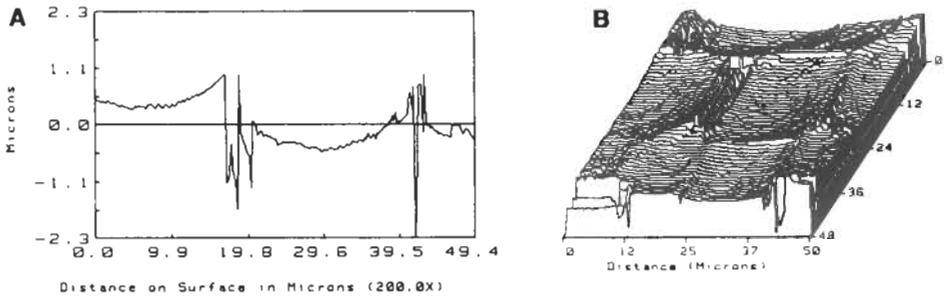Distance on Surface in Microns (200.0X)

B

Figure 3   Optical profiler measurements of a region on the unpolished back of a silicon wafer: line scan (a); and 3D display (b) (Courtesy of WYCO Corp.).

determined by computer calculation using the stored data points for the line scan. A 3D representation, such as the one shown in Figure 3b, adds significantly to the information obtained about the surface from a line scan because crystallographic features can be identified.

In general, optical profilers have the same advantages as mechanical profilers: no sample preparation and short analysis time. However, the optical system also has some disadvantages. If the surface is too rough (roughness greater than 1.5 μm), the interference fringes can be scattered to the extent that topography cannot be determined. If more than one matrix is involved, for example, for multiple thin films on a substrate, or if the sample is partially or totally transparent to the wavelength of the measurement system, then measurement errors can be introduced. Software advances have improved the accuracy of measurements on a single film on a substrate. Even though a phase may be introduced because of a difference in indexes of refraction between the film and the substrate, a correction can be applied. Multiple matrix samples can be measured if coated with a layer that is not transparent to the wavelength of light used.

Scanning Electron Microscope (SEM)

SEM images are formed on a cathode ray tube with a raster synchronized with the raster of an electron beam moving over the sample of interest. Variations in the intensity of electrons scattered or emitted by the sample result in changes in the brightness on the corresponding points on the display. SEM measurements of the surface topography can be very accurate over the nanometer to millimeter range. Specific features can be measured best by cleaving the sample and taking a cross sectional view.

As an example, consider again the back surface of the silicon wafer used in the mechanical profiler example. Figure 4a, an SEM micrograph taken at 45° tilt, shows a surface covered with various sized square-shaped features that often overlap. This information cannot be discerned from the mechanical profiler trace, but can be obtained using a 3D optical profiler measurement. Figures 4b and 4c are also
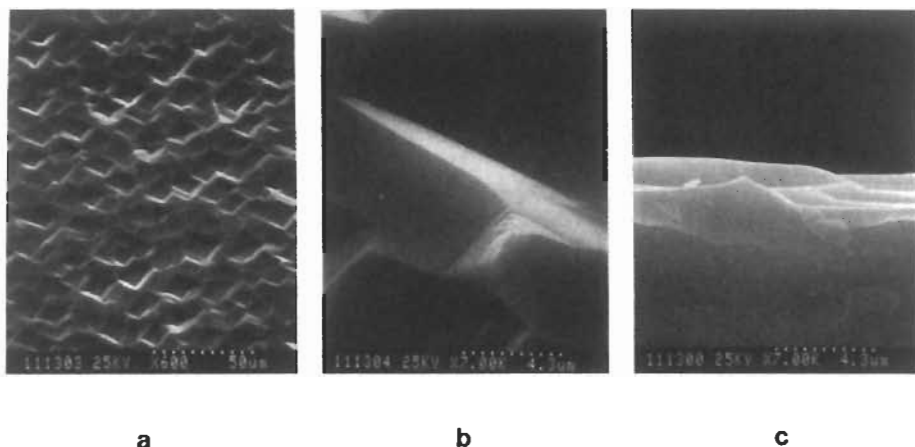
a   b   c

Figure 4   **SEM micrographs of a region on the back of a silicon wafer: (a) and (b) show the surface at different magnifications; (c) is a cross sectional view (Courtesy of P. M. Kahora, AT&T Bell Laboratories).**

SEM micrographs of the same sample. Figure 4b shows an area similar to that of Figure 4a, but at a higher magnification. Figure 4c is a cross sectional view that indicates the heights of several individual features. All three micrographs were taken at relatively low magnification for an SEM. Note that for many types of manufactured silicon wafers, the surface on the back of the wafer undergoes an acid etch after the lapping process and would exhibit a much more random surface roughness. The surface shown in the example results from a potassium hydroxide etch, which causes enhanced etching along certain crystallographic orientations.

Specific SEM techniques have been devised to optimize the topographical data that can be obtained. Stereo imaging consists of two images taken at different angles of incidence a few degrees from each other. Stereo images, in conjunction with computerized frame storage and image processing, can provide 3D images with the quality normally ascribed to optical microscopy. Another approach is confocal microscopy. This method improves resolution and contrast by eliminating scattered and reflected light from out-of-focus planes. Apertures are used to eliminate all light but that from the focused plane on the sample. Both single (confocal scanning laser microscope, CLSM) and multiple (tandem scanning reflected-light microscope, TSM or TSRLM) beam and aperture methods have been employed.

Some disadvantages for SEM measurements, compared with data from mechanical and optical profilers, are that the sample must be inserted into a vacuum system, and charging problems can make the analysis of insulators difficult. SEMs are also much more expensive than profilers.
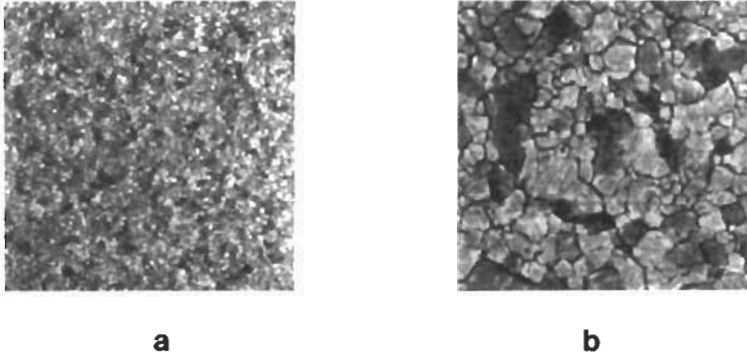
a   **b**

Figure 5   Atomic force microscope images of an aluminum film deposited on ambient
(a) and heated (b) Si substrates. The scales are 15 μm × 15 μm (a) and 20 μm ×
20 μm (b). The grain size can be clearly observed (Courtesy of M. Lawrence A.
Dass, Intel Corporation).

Atomic Force Microscope

An Atomic Force Microscope (AFM), also called a Scanning Force Microscope
(SFM), can measure the force between a sample surface and a very sharp probe tip
mounted on a cantilever beam having a spring constant of about 0.1–1.0 N/ m,
which is more than an order of magnitude lower than the typical spring constant
between two atoms. Raster scanning motion is controlled by piezoelectric tubes. If
the force is determined as a function of the sample's position, then the surface
topography can be obtained.[1, 2] Detection is most often made optically by interfer-
ometry or beam deflection. In AFM measurements, the tip is held in contact with
the sample. Spatial resolution is a few nanometers for scans up to 130 μm, but can
be at the atomic scale for smaller ranges. Both conducting and insulating materials
can be analyzed without sample preparation.

Figure 5 shows AFM images of the surfaces of Al-0.5 % Cu thin films deposited
on unheated (Figure 5a) and heated (Figure 5b) Si substrates. The aluminum grain
size is smaller in the sample deposited at ambient temperature. Root-mean-square
roughness was measured at 5.23 and 7.45 nm, respectively, for the ambient and
heated samples. The depth of the grain boundaries can be determined from a 3D
image. The roughness of the aluminum on the unheated substrate is dominated by
the different grains, but the heated substrate sample roughness is determined by
grain boundaries.

Scanning Tunneling Microscope (STM)

Electrons can penetrate the potential barrier between a sample and a probe tip, pro-
ducing an electron tunneling current that varies exponentially with the distance.

The STM uses this effect to obtain a measurement of the surface by raster scanning over the sample in a manner similar to AFM while measuring the tunneling current. The probe tip is typically a few tenths of a nanometer from the sample. Individual atoms and atomic-scale surface structure can be measured in a field size that is usually less than 1 μm × 1 μm, but field sizes of 10 μm × 10 μm can also be imaged. STM can provide better resolution than AFM. Conductive samples are required, but insulators can be analyzed if coated with a conductive layer. No other sample preparation is required.

Examples of semiconductor applications include the imaging of surface coatings to determine uniformity and the imaging of submicron processed features.

Optical Scatterometry

An optical scatterometer can be used to measure angularly resolved light scatter. The light source for one of the systems in use is a linearly polarized He–Ne laser with the polarization plane perpendicular to the plane of incidence. Light scattered from the sample is focused onto an aperture in front of a photomultiplier. The multiplier is rotated in small increments (< 0.5°) and the scattered light intensity is measured at each point. This method provides a noncontact measurement of roughness for reflecting samples and is capable of determining subsurface damage in silicon and gallium arsenide wafers.[3, 4] Root-mean-square roughness measurements as low as 0.1 nm can be obtained. No sample preparation is required for analysis.

If the sample is fully or partially transparent to the incident beam, light may be scattered from the back of the sample or from within the sample, and the surface measurement will be inaccurate.

Roughness Formed by Sputtering

The sputtering process is frequently used in both the processing (e.g., ion etching) and characterization of materials. Many materials develop nonuniformities, such as cones and ridges, under ion bombardment. Polycrystalline materials, in particular, have grains and grain boundaries that can sputter at different rates. Impurities can also influence the formation of surface topography.[5]

For several analytical techniques, depth profiles are obtained by sputtering the sample with a rastered ion beam to remove atoms from the surface and gradually form a crater. The most common elements used for primary beams are oxygen, argon, cesium, and gallium. For many materials, rastered or unrastered sputtering produces a rough surface. Even single-crystal materials are not immune to ion bombardment-induced topography formation. Ridges have been detected in Si, GaAs, and AlGaAs after O_2^+ bombardment. Figure 6 is a set of SEM micrographs that show the formation of a series of ridges in (100) Si after bombardment to increasing depth with a 6-keV O_2^+ primary beam at approximately 60° from normal inci-

	Mechanical profiler
Depth resolution	0.5 nm
Minimum step	2.5–5 nm
Maximum step	~150 μm
Lateral resolution	0.1–25 μm, depending on stylus radius
Maximum sample size	15-mm thickness, 200-mm diameter
Instrument cost	$30,000–$70,000
	Optical profiler
Depth resolution	0.1 nm
Minimum step	0.3 nm
Maximum step	15 μm
Lateral resolution	0.35–9 μm, depending on optical system
Maximum sample size	125-mm thickness, 100-mm diameter
Instrument cost	$80,000–$100,000
	SEM (see SEM article)
	Scanning force microscope (see STM/SFM article)
Depth resolution	0.01 nm
Lateral resolution	0.1 nm
Instrument cost	$75,000–$150,000
	Scanning tunneling microscope (see STM/SFM article)
Depth resolution	0.001 μm
Lateral resolution	0.1 nm
Instrument cost	$75,000–$150,000
	Optical scatterometer
Depth resolution	0.1 nm (root mean square)
Instrument cost	$50,000–$150,000

Table 1   **Comparison of the capabilities of several methods for determining surface roughness.**

dence.[6] The ridges that develop during this process are perpendicular to the direction of the ion beam. One explanation of the cause of this particular formation is based on the instability of a plane surface to periodic disturbances.[7] Topography
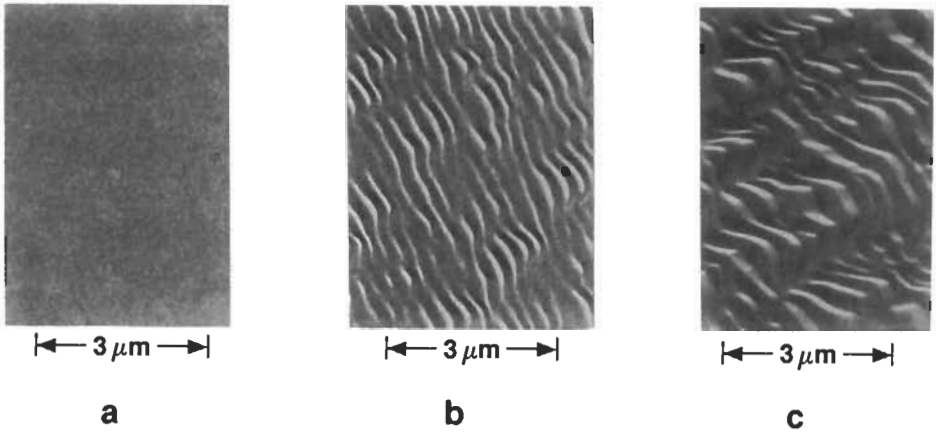
|←— 3 μm —→| |←— 3 μm —→| |←— 3 μm —→|

a   **b**   **c**

Figure 6   **SEM micrographs of the bottoms of SIMS craters in (100) Si after 6 keV O_2^+ bombardment to 2.1 μm (a), 2.8 μm (b), and 4.3 μm (c). The angle of incidence is approximately 40° from normal.[6]**

formation is different for different primary beams and for different angles of incidence. The ridges in Si do not form with Cs^+ bombardment or, at high angles of incidence from the normal, with O_2^+ bombardment.

Impact on Depth Profiling

Depth Resolution and Secondary Ion Yield

Roughness from sputtering causes loss of depth resolution in depth profiling for Auger Electron Spectroscopy (AES), X-Ray Photoelectron Spectroscopy (XPS), and SIMS.

Degraded depth resolution is especially apparent in the case of metals.[8] Figure 7 shows the analysis of a 1-μm film of aluminum on a silicon substrate. The interface between the layer and substrate is smeared out to the extent that only an approximate idea of the interface location can be obtained. The sputtering rates for aluminum and silicon under the conditions used differ by almost a factor of 2. Therefore, the sputtering rate varies significantly in the poorly resolved interface region and the depth axis cannot be accurately calibrated. The roughness at the bottom of the crater can be severe enough to affect the depth measurement of the crater.

For SIMS profiles, the secondary ion yield can also be affected by sputter-induced roughness. Figure 8 shows changes in secondary ion yield for silicon monomeric and polymeric species analyzed under the same conditions as the sample shown in the SEM micrographs from Figure 6. The micrographs correlate with the depths shown on the profile and prove that the change in ion yield is coincident with the topography formation.[6] The ion yield change (before and after topography formation) can vary for each secondary ion species. For the example, in
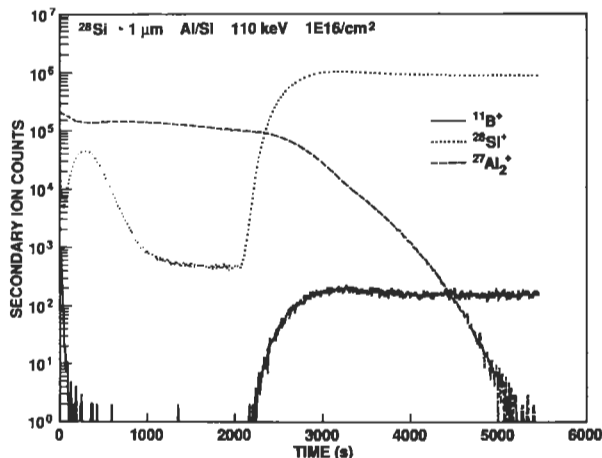
Figure 7 SIMS depth profile of Si implanted into a 1-μm layer of Al on a silicon substrate for 6-keV O_2^+ bombardment. The substrate is B doped.

Figures 6 and 8 the changes were approximately 65 % for $^{28}Si^+$ and over 250 % for $^{16}O^+$. Different ions can have yields affected in opposite directions, as shown by the two species in Figure 8. Other materials, such as GaAs, have also shown significant changes in ion yield that have been correlated with microtopography formation.

Sample Rotation During Sputtering

Corrective action for roughening induced by sputtering has taken several directions. The simultaneous use of two sputtering beams from different directions has been explored; however, rotation of the sample during ion bombardment appears to be the most promising. Attention to the angle of incidence is also important
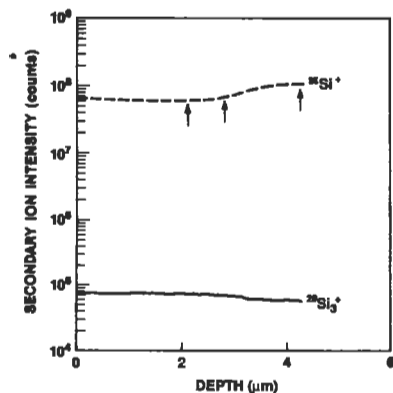

Figure 8 SIMS depth profile of (100) Si for 6-keV O_2^+ bombardment at approximately 40° from normal incidence. The arrows show the depths at which the SEM micrographs in Figure 6 were taken.[6]
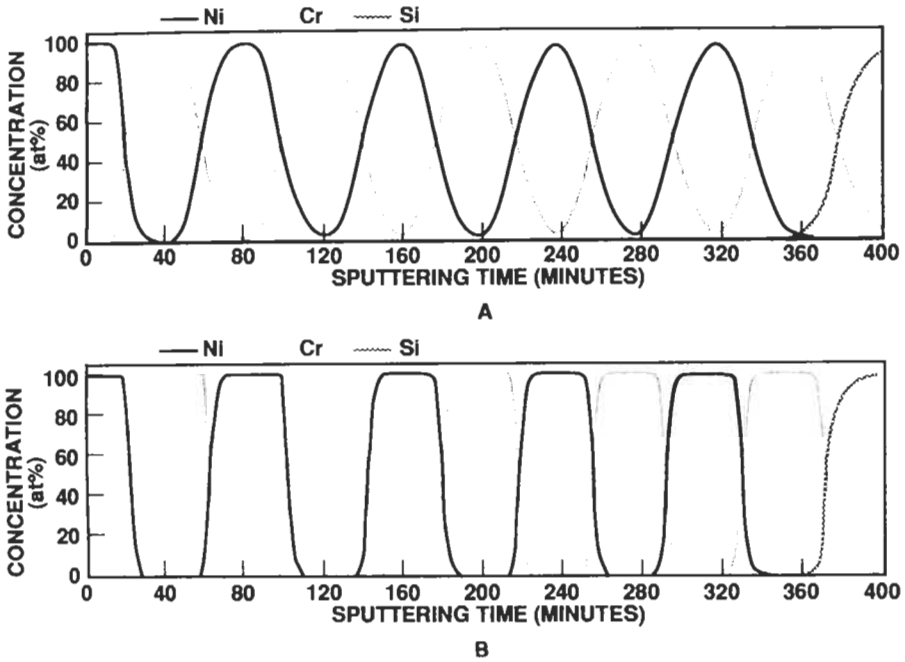
Figure 9 AES depth profiles of multilayer Cr/ Ni thin film structures on a smooth substrate using a 5-keV Ar+ primary beam: without rotation of the sample during bombardment (a), and with rotation (b).[9]

because topography formation can be reduced or eliminated for certain materials if the angle of incidence from the normal is 60° or higher.

If a sample of polycrystalline material is rotated during the sputtering process, the individual grains will be sputtered from multiple directions and nonuniform removal of material can be prevented. This technique has been successfully used in AES analysis to characterize several materials, including metal films. Figure 9 indicates the improvement in depth resolution obtained in an AES profile of five cycles of nickel and chromium layers on silicon.[9] Each layer is about 50 nm thick, except for a thinner nickel layer at the surface, and the total structure thickness is about 0.5 μm. There can be a problem if the surface is rough and the analysis area is small (less than 0.1-μm diameter), as is typical for AES. In this case the area of interest can rotate on and off of a specific feature and the profile will be jagged.

This technique has recently been sucessfully applied to SIMS depth profiling.[10] Figure 10 shows a profile of a GaAs/AlGaAs superlattice with and without sample rotation. The profile without rotation shows a severe loss of depth resolution for the aluminum and gallium signals after about 15 periods, whereas the profile with rotation shows no significant loss of depth resolution after almost 70 periods. The data
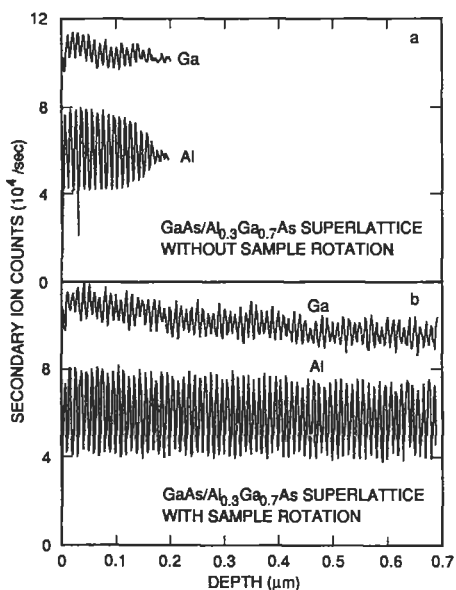
Figure 10 **SIMS depth profiles with and without sample rotation during bombardment by 3-keV O_2^+ at 40° from normal incidence.[10]**

were taken using a 3-keV oxygen primary beam rastered over a 1-mm × 1-mm area at 8 nm/min. The rotation speed was approximately 0.6 cycles/min. Additional work by the same group has shown that the secondary ion yield changes described above are removed also if the sample is rotated.

Related Articles in the Encyclopedia

Dynamic SIMS, AES, SEM, STM, and SFM

References

1 N. A. Burnham and R .J. Colton. *J. Vac. Sci. Technol.* **A7,** 2906, 1989.

2 N. A. Burnham and R. J. Colton. in *Scanning Tunneling Microscopy: Theory and Practice.* (D. A. Bonnell, ed.) V.C.H. Publishers, New York, 1991.

3 R. D. Jacobson, S. R. Wilson, G. A. Al-Jumaily, J. R. McNeil, J. M. Bennett, and L. Mattsson. *Applied Optics.* 1991.

4 J. R. McNeil, et al. *Optical Eng.* **26,** 953, 1987.

5 *Ion Bombardment Modification of Surfaces* (O. Auciello and R. Kelly, eds.) Elsevier, Amsterdam, 1984.

6 F. A. Stevie, P .M. Kahora, D .S. Simons, and P. Chi. *J. Vac. Sci. Technol.* **A6,** 76, 1988.

7 R. M. Bradley and J. M. E. Harper. *J. Vac. Sci. Technol.* **A6,** 2390, 1988.

8 R. G. Wilson, F. A. Stevie, and C. W. Magee. *Secondary Ion Mass Spectrometry: A Practical Handbook for Depth Profiling and Bulk Impurity Analysis.* Wiley, New York, 1989.

9 A. Zalar. *Thin Solid Films.* **124,** 223, 1983.

10 E.-H. Cirlin, J. J. Vajo, T. C. Hasenberg, and R. J. Hauenstein. *J. Vac. Sci. Technol.* **A8,** 4101, 1990.

12.2   Optical Scatterometry

JOHN R. MCNEIL, S.S.H. NAQVI, S.M. GASPAR,
K.C. HICKMAN, AND S.D. WILSON

Contents

- Introduction
- Basic Principles and Applications
- Comparison to Other Techniques
- Conclusions

Introduction

Many technologies involve the need to monitor the surface topology of materials. First the topology itself may be of direct interest. Second, topology is usually strongly influenced by the processing steps used to produce the surface; characterizing the topology therefore can serve as a process monitor. Angle-resolved characterization of light scattered from a surface, or scatterometry, is a very attractive diagnostic technique to characterize a sample's topology. It is noncontact, nondestructive, rapid, and often provides quantitative data. Scatterometry can be used as a diagnostic tool in the fabrication of microelectronics, optoelectronics, optical elements, storage media, and other, less glamorous areas such as the production of paper and rolled materials. Application of scatterometry in some cases eliminates the need for microscopic examination. The technique is amenable to automated processing, something which is not possible using microscopic examination.

Basic Principles and Applications

The arrangement illustrated in Figure 1 is commonly used for angular characterization of scattered light. The light source is usually a laser. The incident beam may be unpolarized, or it can be linearly polarized with provisions for rotating the plane of polarization. Typically the plane of polarization is perpendicular to the plane of
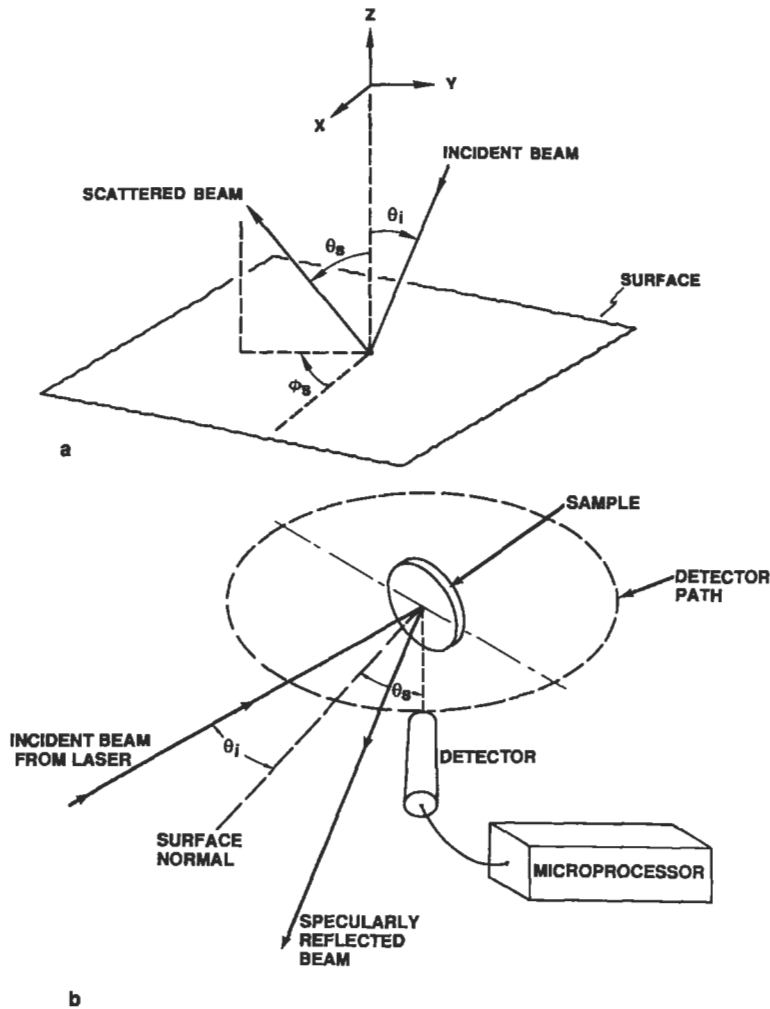
Figure 1 Scatterometer arrangement, illustrating the geometry (a) and the experimental configuration (b).

incidence (s-polarized light), as this avoids surface plasma wave coupling in conducting samples. The laser output is spatially filtered to provide a well-defined spot at the sample. This is critical for allowing measurements close to the specularly reflected beam or the directly transmitted beam (in the case of a sample which is transmitting at the wavelength of interest); the significance is described below. Sometimes the detector also has provisions for polarization discrimination. The detector is typically a photomultiplier or a Si photodiode. Other detection arrangements include multiple detectors or diode arrays. Arrangements that employ cam-

era and screen configurations recently have shown utility for measuring scattering in two dimensions. Theoretical aspects of light scattering are reviewed below in connection with applications.

Applications of scatterometry can best be described by considering two general categories of surfaces that are examined: surfaces which are nominally smooth, and surfaces which are intentionally patterned. In the first category, scatterometry is used to measure surface roughness and other statistical properties of the sample's topology. Certain conditions of the surface are assumed, and these are discussed below. In addition, for some "smooth" surfaces, such as optical components, the scattered light intensity itself is the item of interest, and little or no additional interpretation is needed. This information might be sufficient to predict the performance of the sample, such as characterizing scattering losses from laser cavity elements.[1-4] Measuring light scattered from intentionally patterned surfaces is a very convenient process monitor in manufacturing areas like microelectronics and optoelectronics. This is an area of active research, with some results now appearing in manufacturing environments.[5-7]

Smooth Surfaces: Surface Topology Characterization

The relation between scattering of electromagnetic radiation and surface topography has been studied for many years, originally in connection with radar. In general this relationship is complicated. However, the relation is simple in the case of a clean, perfectly reflecting surface in which the heights of the surface irregularities are much smaller than the wavelength of the scattered light (i.e., the smooth-surface approximation). We present the results of Church's treatment.[2]

Vector scattering theories describe the differential light scatter dI_s as

$$\frac{1}{I_i}\left(\frac{dI_s}{d\omega_s}\right) = \frac{C}{\lambda^4} Q(\theta_i, \phi_i, \theta_s, \phi_s, N, \chi_i, \chi_s) P(p, q) \tag{1}$$

where C is a constant, I_i is the intensity of the incident light, and $d\omega_s$ is the solid angle of the detection system. The quantity Q in Equation (1), called the *optical factor*, is independent of the surface condition and is a function of the angles of incidence (θ_i, ϕ_i), the scattering angles (θ_s, ϕ_s), complex index of refraction N of the surface, and polarization states of the incident and scattered light, χ_i and χ_s, respectively. The *surface factor* $P(p, q)$ is the power spectral density of the surface roughness; it is the output of the scatterometer measurement and is the function which describes the surface structure.

If the surface (i.e., the best fit plane) is in the x–y plane, and $Z(x, y)$ is the surface height variation (surface roughness) relative to that plane, the power spectral density is given by

$$P(p, q) = \frac{1}{A}\left[\frac{1}{2\pi}\iint dxdy e^{i(px+qy)} z(x, y)\right]^2 \qquad (2)$$

where A is the area of the scatterer, and p and q are the surface spatial frequencies in the x- and y-directions, respectively. In other words, the power spectral density is the average squared magnitude of the two-dimensional Fourier transform of the surface roughness.

Although the power spectral density contains information about the surface roughness, it is often convenient to describe the surface roughness in terms of a single number or quantity. The most commonly used surface-finish parameter is the root-mean-squared (rms) roughness σ. The rms roughness is given in terms of the instrument's band width and modulation transfer function, $M(p, q)$ as

$$\sigma^2 = \int_{p_{min}}^{p_{max}} dp \int_{q_{min}}^{q_{max}} dq M(p, q) P(p, q) \qquad (3)$$

Different values of σ^2 will result if the integral limits (i.e., band width) or modulation transfer function in the integral change. All surface characterization instruments have a band width and modulation transfer function. If rms roughness values for the same surface obtained using different instruments are to be compared, optimally the band widths and modulation transfer functions would be the same; they should at least be known. In the case of isotropic surface structure, the spatial frequencies p and q are identical, and a single spatial frequency (p) or spatial wavelength ($d = 1/p$) is used to describe the lateral dimension of structure of the sample.

An intuitive understanding of the power spectral density can be obtained by considering the surface to be composed of a number of surfaces, each having structure of a single spatial frequency that is sinusoidally varying in amplitude (height). Measuring the scattered light at a specific scattering angle corresponds to characterizing structure of a specific spatial frequency, and the intensity of the scattered light is proportional to the amplitude of the structure. The situation is analogous to Fourier analysis of an electrical signal. Figure 2 illustrates this idea by comparing polished Cu and Mo surfaces. The micrograph of the Cu surface in Figure 2a shows the dominance of fine texture and lines (high spatial frequency structure) which result from polishing the soft material. By contrast, the hard Mo surface has relatively little fine structure and is dominated by wide regions due to the large grains of the material. The two power spectral density characteristics shown in Figure 2b are a quantitative description of the information in the micrographs.

The modulation transfer function of the optical scatterometer is nearly unity.[4] The spatial frequency band width, using 0.633-nm photons from a He–Ne laser, is typically 0.014–1.6 μm^{-1}, corresponding to a spatial wavelength band width 70–0.633 μm. This corresponds to near normal sample illumination with a minimum

POLISHED Cu   POLISHED Mo

a

b   SPATIAL FREQUENCY (μm^{-1})
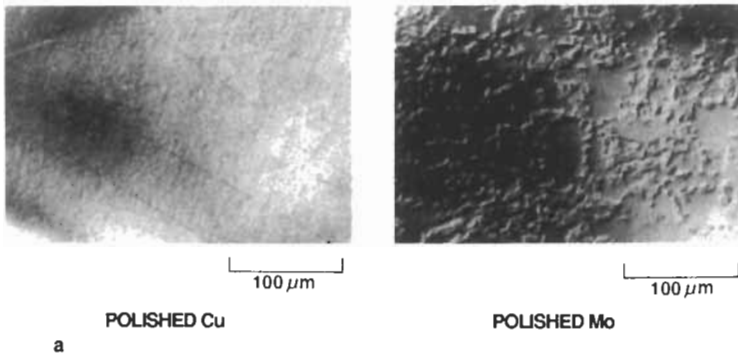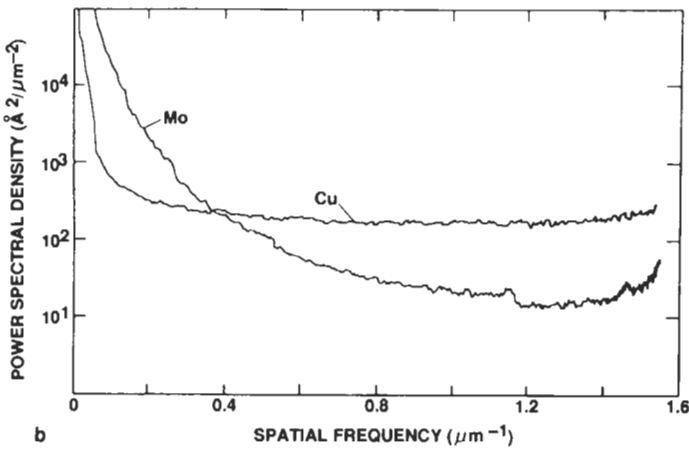
Figure 2   **Comparison of two polished metal surfaces: (a) photographs from Nomarski microscope examination; and (b) power spectral density characteristics of the same surfaces.**

scattering measurement angle of 0.5° from the specular beam. Measurements closer to the specular extend the 70-mm limit to larger values. For nonnormal angle of incidence these limits shift to smaller values. Similarly, a larger optical wavelength shifts these limits to larger values. This behavior is determined by the grating equation,

$$\sin\theta_s = \sin\theta_i + \frac{n\lambda}{d} \qquad (4)$$

where $n = \pm1, \pm2$, and so forth. For smooth surfaces, only the first order is considered.

The importance of instrument band width is illustrated by considering the rms roughness of the two samples of Figure 2. If the rms roughness is calculated over the

band width 0.014–1.6 μm^{-1}, the roughness of the Mo sample is approximately 85 Å, and that of the Cu sample is 35 Å. The same power spectral density characteristics can be analyzed over a smaller band width, 0.06–1.6 μm^{-1}, and both surfaces have an rms roughness of approximately 30 Å. It is important to know these widths because all surface roughness measurement techniques have band widths.

The technique described above has been applied to characterize morphology of optical components[4] and microelectronics materials.[1] In the latter, an Al–Si (2%) alloy material was characterized that had been deposited at different substrate temperatures. The material grain size was determined using SEM inspection and was found to be highly correlated with the rms roughness results from the scatterometer characterization. This makes the scattering technique appear useful for grain-size analysis of this material, thus providing the analysis normally obtained using SEM inspection. Characterization of CVD W and WSi_2 is described in Gaspar et al.[1]

The preceding discussion relates only to a perfectly reflecting surface. If the surface transmits the incident light, either completely or only a short distance, the scattered light originates from the volume that is illuminated, as well as from the front surface and back surface (if illuminated). In this situation, the preceding treatment is not applicable, and analysis of the data is not straightforward. However, the technique still can provide very useful information on sample morphology. In general, the high spatial frequency structure of a surface or in the volume of the sample will scatter primarily at large angles. However, multiple scattering events in the material complicate the situation.

Smooth Surfaces: Characterization of Sample Bidirectional Scattering Distribution Function

The light scattered from a sample can fill the entire 4π steradians of space if the sample is transparent at the wavelength of interest, and 2π steradians if it is not. The angular distribution is a function of the optical properties (index, homogeneity, orientation, etc.), surface roughness and contamination of the sample, polarization of the source, and angles of incidence and detection. The bidirectional scattering distribution function (BSDF) is the term commonly applied to describe this pattern, and it is simply defined in radiometric terms as the ratio of the scattered surface radiance, measured at angle θ_s, to the incident surface irradiance. The former is the light flux or power P_s (Watts) scattered per unit surface area of the sample illuminated, per unit projected solid angle of the detection system. The incident surface irradiance is the light flux Pi (Watts) on the surface per unit of illuminated surface area. The projected solid angle is the solid angle $d\omega_s$ of the detection system times $\cos(\theta_s)$. BSDF is expressed as

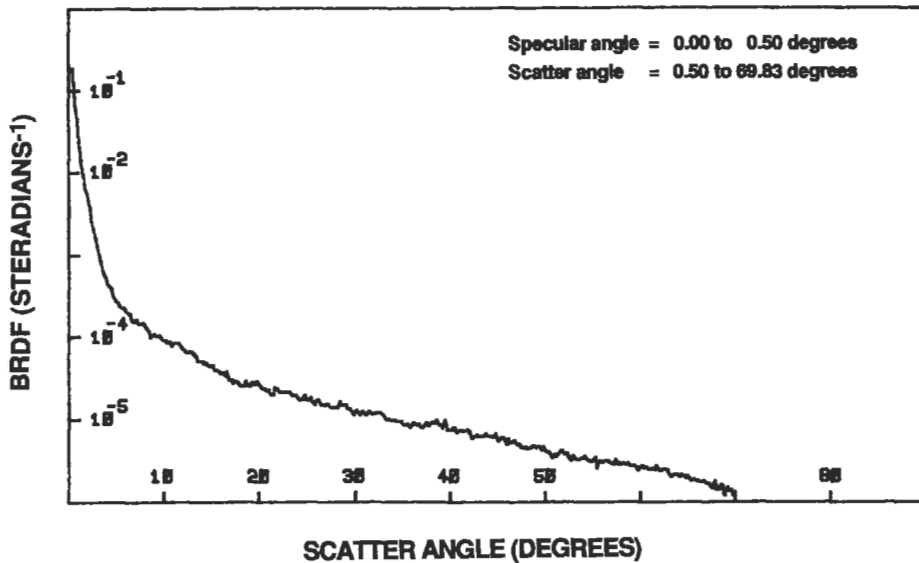$$BSDF = \frac{dP_s/d\omega_s}{P_i \cos\theta_s} \tag{5}$$

Figure 3   Example of the BRDF characteristic of a polished optical surface. Note the rapid increase in scattering at small scatter angles.

This expression for BSDF is appropriate for all angles of incidence and all angles of scatter, and it has units of (steradians^{-1}). Note that this expression was originally derived by Nicodemus, who assumed a plane wave input for the source beam. If BSDF is measured on the same side of the sample as the incident light source, the scattering characterization is referred to as bidirectional reflectance distribution function (BRDF); if scattering is measured on the other side of the sample, it is referred to as bidirectional transmittance distribution function (BTDF). Note that BRDF can have very large values. For example, when the specular reflection is measured, P_i/P_s is nearly unity, and BRDF is approximately $1/\omega_s$, which can be very large (e.g., 10^4). BRDF can be viewed as the directional reflectance of the sample per steradian. Note, too, that the factor $\cos\theta_s$ is sometimes not included in the expression above for BSDF, in which case it is said to be no longer "cosine corrected."

As discussed previously, BSDF characteristics of a sample depend strongly on the incident angles (θ_i, ϕ_i) and scattering measurement angles (θ_s, ϕ_s); in general they both increase very rapidly as scattered light measurements are made closer to the directly transmitted beam (BTDF) and the specularly reflected beam (BRDF). Figure 3 illustrates this by showing a typical BRDF characteristic of a polished optical surface.

Intentionally Patterned Surfaces

High technology surfaces (e.g., microelectronics) are often intentionally patterned, and light scattering may be used for subsequent characterization of the pattern. In

particular, the pattern can be a structure that is periodic in one or more directions. The pattern may be a device of interest in a fabrication process, or it might be an imposed test pattern such as a diffraction grating. Light is diffracted (scattered) into several distinct orders as described by the grating equation. The intensity of the light in the different orders is a very sensitive function of the shape of the lines of the pattern. If the shape of the lines of the pattern is influenced by a processing step, scattering characterization can provide a simple way to monitor the process.

This technique has been used recently [5-7] to provide an attractive, simple monitor of processes involved in microelectronics fabrication. Sub-μm-wide lines of metal on glass used in photomasks have been accurately measured. The technique has been applied to characterize the depth and side wall angle of etched microelectronics structures. It also has been used to directly monitor the exposure level in photoresist during lithography for microelectronics processing. The technique has been used for noncontact temperature measurement of surfaces at room temperature and at elevated (700° C) temperatures; 1° C resolution has been achieved. Other applications to microelectronics and storage media are underway, and it is very realistic to expect this type of scattering characterization to develop into a valuable process monitor for use in many technological areas.

Theoretical modeling of the process consists first of predicting the fraction of incident power diffracted into the different orders by illuminating a known structure. The power distribution is a function of the shape of the lines in the periodic structure and is somewhat application specific. For example, in the case of trapezoidal shaped lines, the parameters of interest are the top line width, the side wall angle, and the height of the line structure. However, all problems involve application of Maxwell's equations in a rigorous vector diffraction approach to calculate this power distribution. A sufficient number of calculations are performed for different values of the line shape parameters of interest to facilitate addressing the inverse of this situation, namely identifying an unknown structure based upon its scattering characteristic. We have used neural network and linear statistical prediction techniques to compliment the theoretical calculations, so that an estimate of the line shape parameters can be obtained from experimentally measured diffracted intensities. This approach has been used successfully in the three applications given above.

Practical Considerations

Several practical issues of the scatterometer must be considered in the case of characterizing nominally smooth surfaces. The incident laser beam may be collimated, but more commonly it is brought to a focus at a distance defined by the arc in which the detector rotates. In addition, a deflection mirror or an optical fiber might be used to direct light to the detector element. These features permit measurements close to the specular and transmitted beams, and this is critical to fully characterize the scattered light. This is especially significant since the scattered light intensity

can change several orders of magnitude within the first few degrees from the specular and transmitted beams. This is illustrated below in connection with sample data. It is important to perform a sufficient number of measurements to fully characterize the scattered light in this region of rapid change.

Another practical concern is the amount of light scattered by the optical elements of the scatterometer system. This instrument scatter, or *signature* can limit the scatterometer sensitivity (e.g., the minimum rms roughness that is measurable). Typically measurements can be performed at minimum scattering angles, $\theta_s = 0.5°–1.0°$, from the specular and transmitted beams without the instrument signature being a concern. The instrument signature is a concern, however, when the intensity of light scattered by the instrument at a particular angle is comparable to the light scattered from a sample.

An additional concern involves how isotropically light is scattered from a sample. If the sample has nonisotropic structure (surface or volume), light will be scattered nonisotropically with respect to ϕ_s (see Figure 1). Examples of surfaces that have nonisotropic structure include fine diffraction gratings, machined parts, computer hard disks, and microelectronics circuits. In some instances it is important to fully characterize scattered light, such as in determining the roughness of machined parts. In this case, the scattering measurements might be performed in several planes. However, this involves complicated instrumentation. Alternatively, the scattered light might be measured in a single plane, as illustrated in Figure 1, and the sample can be rotated about a normal axis passing through the point of illumination. Allowance must be made for rotating the polarization of the input beam to maintain the appropriate geometry.

A final practical note involves instrument intensity measurement calibrations. The intensity measurement is self-calibrating relative to the incident beam from the source. However, measurements typically have a dynamic range of $10^8–10^{10}$, and care must be taken to insure the detection system is linear. A method of calibrating the scatterometer is to characterize a diffuse reflector having a known scattering characteristic. For example, a surface coated with $BaSO_4$ makes a nearly Lambertian scatterer, which has a BRDF of $1/\pi$ at all angles.

Comparison to Other Techniques

Other methods available to characterize surface topology include optical and mechanical profilometers, and microscopy techniques. These techniques suffer from some combination of being contact, destructive, sensitive to vibration, qualitative, or slow to apply. Light scattering techniques avoid these. Another aspect of comparison has to do with the utility of a technique in advanced manufacturing environments. In particular, microscopy and profilometry techniques are not amenable to *in-situ* use, and this is a deterrent for their application as real-time, on-line process monitors. Scatterometers can be incorporated into many processing arrangements for *in-situ* use. This provides rapid feedback for process control. In

addition, the scatterometer is available in rugged, user-friendly forms that can be operated by unskilled personnel.[8]

In the case of scatterometry applications mentioned above in connection with patterned surfaces, there are sometimes no alternative characterization techniques. For example, there currently is no direct monitor of photoresist exposure dose for lithography in microelectronics processing. This is very significant, as a Si wafer typically spends up to 50% of its processing time in lithography. There is no alternative to noncontact temperature measurements having the resolution and temperature range of the scattering technique described above; these are requirements for advanced processing of microelectronics.

The significance of instrument band width and modulation transfer function was discussed in connection with Equation (3) to characterize the roughness of nominally smooth surfaces. The mechanical (stylus) profilometer has a nonlinear response, and, strictly speaking, has no modulation transfer function because of this. The smallest spatial wavelength which the instrument can resolve, d_{min}, is given in terms of the stylus radius r and the amplitude a of the structure as

$$d_{min} = 2\pi\sqrt{ar} \qquad (6)$$

This expression is applicable for a surface consisting of a single spatial frequency and is discussed in detail in Wilson et al.[9] Stylus curvatures of 12 μm are often used, and smaller curvatures are available. For a 12-μm curvature stylus to have a lateral resolution of 1 μm, the amplitude of the structure cannot exceed 20 Å, or the stylus will not follow the contour of the surface; to resolve 0.6 μm the amplitude cannot exceed 7.4 Å. A lateral resolution of 500 Å is quoted by some stylus instrument manufacturers. In this case the surface amplitude could not exceed 0.6 Å, using a 1-μm stylus, and 0.05 Å, using a 12-μm stylus. These surface amplitudes are clearly unrealistic. The presence of multiple spatial frequencies (i.e., realistic surfaces) causes harmonic distortion and other nonlinear effects. The long spatial wavelength limit of the band width is determined by the scan length of the stylus, with hundreds of μm being easily achievable. This limit is somewhat larger than that of the scatterometer. In general, using the stylus profilometer to profile a surface is valid only when the surface wavelengths are large compared to the stylus radius, and amplitudes are small compared to the radius. However these instruments are very useful for measuring step heights, the purpose for which they were originally designed.

Optical profilometers have nonlinear modulation transfer function characteristics resulting from an arrangement involving an incoherent imaging system.[4] Results from characterizing surfaces using an optical profilometer are compared to those from scatterometer and stylus measurements and discussed in Jacobson et al.[4] The optical profilometer equipped with a 20× objective lens has a short spatial wavelength resolution limit of approximately 2 μm and a long wavelength limit of

approximately 160 μm. If the optical profilometer is used to profile a surface that has transparent thin films, the optical and mechanical "surfaces" will not necessarily be the same.

When using microscopy techniques to obtain topology information one must be aware of the spatial wavelength band width of the instrument, and this obviously depends on the instrument's magnification. In general the short spatial wavelength (resolution) limit of STM, AFM, SEM, and TEM techniques can be many times smaller than that of scatterometry. Because of this, applications of these techniques are sometimes very different from those of scatterometry, even though they involve characterizing topology or morphology. Instrument modulation transfer function can depend on a number of aspects of the instrument. For example, the STM and AFM probe characteristics strongly influence instrument response. Other microscopy techniques have less quantitative vertical resolution.

Conclusions

Light scattering techniques will play an increasingly significant role in materials processing, especially from surfaces that are intentionally patterned. Visible wavelength light has been used to easily characterize structures having a line width of 0.3 μm. Shorter wavelength laser output can be used to probe even smaller features. The technique is noncontact, nondestructive, noncontaminating, rapid, and it often yields quantitative measurements of surface structures. Future applications will include using the technique as an *in-situ* diagnostic tool.

Related Articles in the Encyclopedia

AFM, Optical Microscopy, STM, and Surface Roughness

References

1   S. M. Gaspar, K. C. Hickman, J. R. McNeil, R. D. Jacobson, Y. E. Strausser, and E. R. Krosche. Metal Surface Morphology Characterization Using Laser Scatterometry. In: *Proceedings of the Spring Meeting of the Materials Research Society.* MRS, 1990. Results are presented of scatterometer characterization of microelectronics materials, including Al-Si, CVD W, and WSi$_2$.

2   E. L. Church, H. A. Jenkinson, and J. M. Zavada. Relation Between the Angular Dependence of Scattering and Microtopographic Features. *Opt. Eng.* **18,** 125, 1979. This article presents an analysis of the relation between angle-resolved light scattering and surface topology.

3   J. C. Stover. *Optical Scattering: Measurement and Analysis.* McGraw-Hill, New York, 1990. This is a good presentation of angle-resolved optical scat-

tering technology, directed primarily toward characterization of optical surfaces.

4 R. D. Jacobson, S. R. Wilson, G. A. Al-Jumaily, J. R. McNeil, and J. M. Bennett. Microstructure Characterization by Angle-Resolved Scatter and Comparison to Measurements Made by Other Techniques. To be published in *Appl. Opt.* This work discusses the band width and modulation transfer function of the scatterometer, stylus profilometer, optical profilometer, and total integrated scattering systems, and gives results of measuring several surfaces using all techniques.

5 S. S. H. Naqvi, S. M. Gaspar, K. C. Hickman, and J. R. McNeil. A Simple Technique for Linewidth Measurement of Gratings on Photomasks. *Proc. SPIE.* **1261,** 495, 1990. K.P. Bishop, S.M. Gaspar, L.M. Milner, S.S.H. Naqvi, and J.R. McNeil. rasterization using Scatterometry. Proc. SPIE. **1545**, 64, 1991. These papers discusses a simple application of scattering from surfaces that are intentionally patterned.

6 K. C. Hickman, S. M. Gaspar, S. S. H. Naqvi, K. P. Bishop, J. R. McNeil, G. D. Tipton, B. R. Stallard, and B. L. Draper. Use of Diffraction From Latent Images to Improve Lithography Control. Presented at the SPIE Technical Conference 1464: Symposium on I.C. Metrology, Inspection, and Process Control, San Jose, CA, 1991, Proc. SPIE. 1464, pp. 245-257, 1991. Another application is presented of scattering characterization and modeling from periodic structures for process control.

7 K. P. Giapis, R. A. Gottscho, L. A. Clark, J. B. Kruskal, D. Lambert, A. Kornblit, and D. Sinatore. Use of Light Scattering in Characterizing Reactively Ion Etched Profiles. To be published in *J. Vac. Sci. Technol.* 1991. This article gives a description of scattering measurements made to characterize line profiles of structures reactively etched in Si.

8 Sandia Systems Inc., Albuquerque, NM, and TMA Technologies, Inc., Bozeman, MT. Sandia systems specializes in systems for characterizing microelectronics and magnetic disk materials; TMA emphasizes optical materials characterization.

9 S. R. Wilson, G. A. Al-Jumaily, and J. R. McNeil. Nonlinear Characteristics of a Stylus Profilometer. *Opt. Eng.* **26,** 953, 1987. This describes modeling stylus profilometer response characteristics and explains their shortcomings.

12.3 MOKE

Magneto-optic Kerr Rotation

DAVID E. FOWLER

Contents

- Introduction
- History and Basic Principles
- Instrumentation
- Comparison With Other Techniques
- Conclusions

Introduction

The magneto-optic Kerr effect (MOKE), or Kerr rotation, provides a simple and straightforward optical method for magnetically characterizing the near-surface region of magnetic materials. Visible, linearly polarized light is reflected from a sample's surface and small rotations in the polarization and small changes in the ellipticity of the light are observed as schematically shown in Figure 1. Elliptical polarization of light results when the two orthogonal components of a light wave's electric field vector have a phase difference. These optical effects result from the interaction of the incident light with the conduction electrons in the magnetic solid. The magnitude of the rotation of the polarization is directly proportional to the net magnetization M of the material reflecting the light. Additionally, MOKE measurements can be used to determine the direction of magnetization in the domains of the material, i.e., for magnetic domain imaging, since the magnitude and sign of the rotation in polarization depends on the relative orientation of the plane of incidence, the incident angle of the light, and the orientation of M. While the amount of rotation is small, typically $\leq 0.5°$, it is well within the detection limits of simple optical hardware.
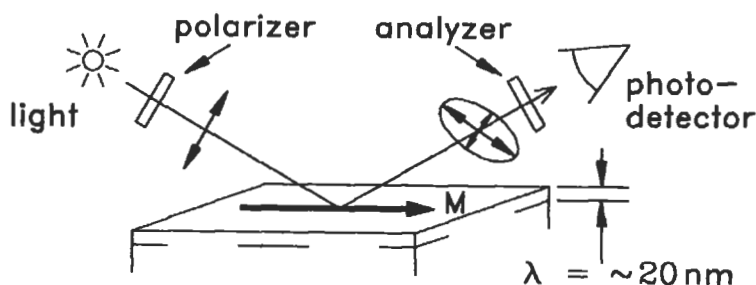
Figure 1 **Schematic diagram showing the basic elements of a MOKE experiment. The angle of incidence, the wavelength of the light, and the orientation of the magnetization, M, relative to the plane of incidence are variables in the experimental setup.**

Since MOKE is an optical probe, its lateral resolution is governed by the diffraction limit of the light source, from 0.3 μm to 0.5 μm for typical wavelengths. Its probing depth is determined by $I/I_0 = \exp(-t/\lambda)$, where the reflected light intensity from a given depth I_0 is attenuated to I for an optical path length t from the surface due to light absorption in the medium; the *absorption* is scaled by a characteristic attenuation length called the optical skin depth λ. For metals, which are good conductors, λ is of the order of 10–20 nm at visible frequencies. As a consequence of the fairly long probing depth of MOKE at optical wavelengths, it can be used to analyze ferromagnetic layers buried by 10 nm or so of an absorbing, nonmagnetic overlayer. Of course, there is no difficulty in obtaining Kerr-related signals from ferromagnetic layers that have been covered by transparent overlayers or vacuum isolated and examined through windows. Under some conditions these intervening transparent layers contribute to the ellipticity of the transmitted light. In fact, this effect can be used to an advantage by appropriately tuning the dielectric properties of the transparent layer to completely compensate the Kerr ellipticity. This results in an enhanced Kerr rotation,[1] which is used extensively in magneto-optic recording technology. For samples where the magnetic material has thickness $d \gg \lambda$ the technique is generally referred to as MOKE, whereas for $d \ll \lambda$ the acronym SMOKE (for *surface* MOKE) is sometimes used. This distinction highlights two important points for ultrathin-film Kerr analysis. First, while the Kerr effect is not intrinsically surface sensitive on the scale of many electron spectroscopies (which have signal attenuation lengths of 0.5–4 nm) it is, in effect, surface sensitive if the magnetic material is confined to the first few atomic layers of a sample, since the Kerr signal is only derived from the magnetic layers. Second, while the rotation of polarization is proportional to M of the magnetic material, it is also strongly influenced by the dielectric properties of the substrate,[2] as is described below.

The MOKE technique has a broad range of applications from the analysis of ultrathin films (less than about 2 nm) to the analysis of the near-surface region of bulk ferromagnets:

1 Hysteresis loops *M–H* have been determined for single atomic monolayers[3] of Fe and Ni that were prepared and measured in ultrahigh vacuum.

2 Maps of the remanent magnetic domain pattern in the near-surface region of magnetic material and thin films can be made routinely.

3 Dynamic domain imaging or Kerr microscopy of low coercivity thin films at MHz domain-switching frequencies allows one to examine domain wall motion in detail.[4]

4 The technology of magneto-optic recording is based on measuring the MOKE signal from remanently magnetized domain patterns in buried magnetic layers.

5 The electron–photon coupling that forms the microscopic basis of MOKE makes it possible, in principle, to determine the electron spin-dependent band structure of elements and alloys.[5] This is done by examining the dependence of the Kerr response on the wavelength of the incident light.

From a practical sense, MOKE is a versatile technique: it is an optical method; the polarization measurement is fairly easy to do; the necessary optical components are common and relatively inexpensive; and it has no intrinsic vacuum requirements.

History and Basic Principles

The first magneto-optic effects were discovered in transparent paramagnetic materials in the presence of a magnetic field by Faraday in 1846. He observed a rotation of polarized light transmitted through the material that depended on the magnitude of an axial magnetic field. This effect is generally quite small, on the order of 1°/cm of material in 10^4 gauss. Later, the polarization rotation of transmitted light through ferromagnetic films was measured and found to be large, on the order of 300,000°/cm in Fe, for example. In 1876, Kerr observed a rotation of the polarization of light reflected from a ferromagnetic surface. Kerr also discovered an electro-optic effect that bears his name, but it is unrelated to the magneto-optic effect of interest here. The Faraday and Kerr magneto-optic effects manifest themselves in a rotation of the polarization of the incident light and in a change in the ellipticity of the polarization upon interaction with a magnetic material. For the purposes of this discussion, it is convenient to describe linearly polarized incident light with components perpendicular to the plane of incidence, generally called *s*-light or *s*-polarized light, and parallel to the plane of incidence, generally called *p*-light or *p*-polarized light. The changes in polarization upon reflection are described schematically in Figure 2 for the case of incident *p*-polarized light. The signs of the rotation and the
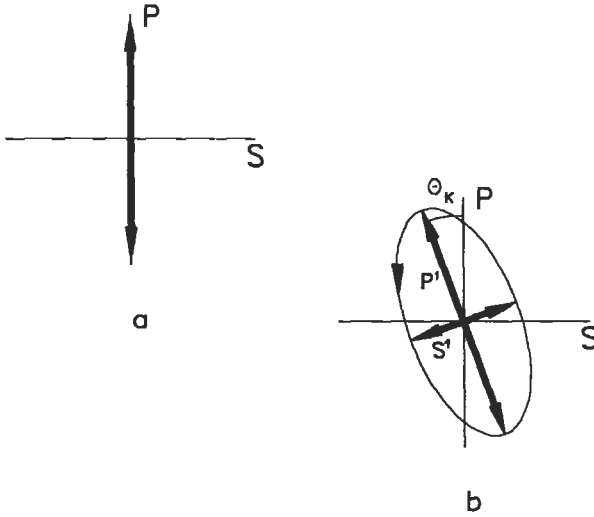
Figure 2   Projection of the time-dependent *E*-field vector of light in the plane transverse to the direction of propagation for linearly polarized light (a), as for incident *p*-light in MOKE, and rotated and elliptically polarized light (b), which is the general case for light reflected from a Kerr-active surface.

ellipticity changes invert when the magnetization of the sample is reversed. The measured rotation is given by θ_K and the ellipticity is $\varepsilon_K = \tan(S'/P')$, as defined in Figure 2.

The macroscopic optical analysis[6] of these effects requires the introduction of two complex indexes of refraction for the ferromagnetic material, one for left-circularly polarized light and another for right-circularly polarized light, which to first order, are given by

$$N_{(r,l)} \approx n \mp \frac{iQ}{2n} \qquad (1)$$

Here, n is the complex index of refraction for the ferromagnet in the paramagnetic state, i.e., above the Curie temperature, and Q is the complex Kerr component. Since any polarization condition, including linearly polarized light, can be described as a linear combination of left- and right-circularly polarized light, the expected rotation and ellipticity of light reflected from a ferromagnet can be determined from standard solutions of the optics wave equations, using the appropriate boundary conditions for the structure of the sample and appropriate, known values for n and Q. In general, both n and Q must be measured for the material of interest. The result of this analysis for the highly symmetric case in which the light is nor-
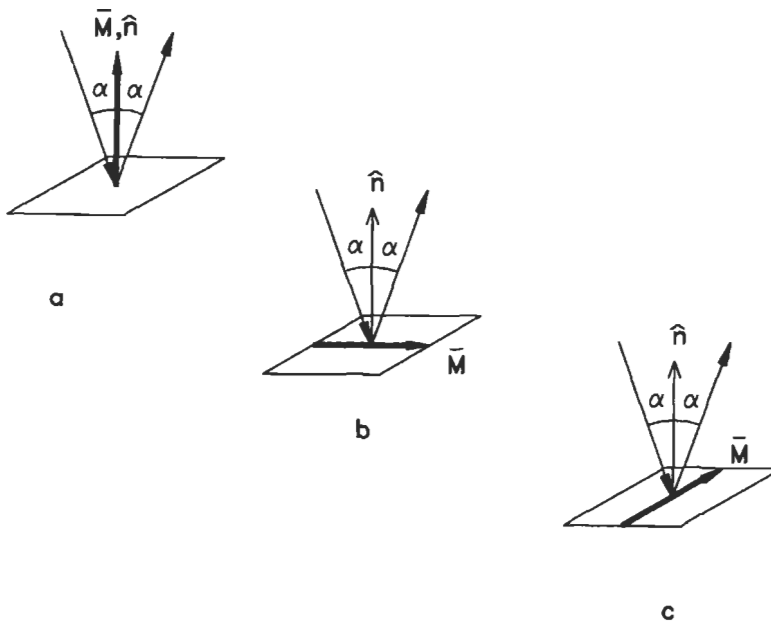
Figure 3   **MOKE geometries for light incident at an angle α with respect to the sample normal $\hat{n}$: polar geometry (a), longitudinal geometry (b), and transverse geometry (c).**

mally incident and the magnetic field is normal to the surface (polar geometry) gives

$$\Phi_K = \theta_K - i\varepsilon_K \approx \frac{-iQ}{n(n^2 - 1)} \tag{2}$$

for the Kerr effect response. Two important conclusions can be drawn from the these results. First, a rearrangement of the preceding relationships for θ_K and ε_K show that there is no MOKE activity when there is no absorption in the magnetic medium, i.e, when n and Q are real. Second, the magnitude of the Kerr rotation depends on the optical dielectric properties of the medium in the near-surface region, as well as on the Kerr activity.

Analyses and results for other geometries are more complicated and will be discussed only qualitatively. The general case of light reflected from a magnetized surface always can be reduced to combinations of the polar geometry, and two other special cases, the longitudinal (or meridional) geometry, and the transverse (or equatorial) geometry. The geometries of all three cases are defined in Figure 3.

From the solutions of the optical wave equations for these boundary conditions, the following statements can be verified;

1 There is no MOKE response for normally incident p- or s-light in either the longitudinal or transverse geometries.

2 There is no MOKE response for pure s-light for any angle of incidence in the transverse geometry.

3 There is no Kerr rotation or Kerr ellipticity for pure p-light or for mixed s- and p-light in the transverse geometry, but there is a magnetization induced change in the surface reflectivity.

4 There is a larger MOKE response at normal incidence for the polar geometry than for oblique angles.

5 There is a larger MOKE response as the angle of incidence becomes more oblique for the longitudinal geometry up to a maximum at an angle of 60° to 80°, depending on the specific material.

The longitudinal Kerr response versus angle is observed to be a slowly varying function with a broad maximum, and there is substantial variation in the angle for the maximum Kerr response reported in the experimental literature.[7] It is useful to note some other practical considerations regarding MOKE measurements. Since the reflectivity of p-light from metals is lower than that of s-light,[8] it is usually the case that the measured Kerr rotations are larger for incident p-light. The maximum MOKE response in the polar geometry is typically found to be 3–5 times greater than the maximum MOKE response for the other two geometries for a given material. The magnitude of the MOKE response has a wavelength dependence that results from the different possible intraband and interband transitions excited in a material's electronic band structure by a given wavelength of light. Some effort has been devoted to obtaining the magnetic band structure of a material through interpretation of the Kerr wavelength dependence. The information is complementary to magnetic band maps derived from spin-resolved photoemission.[9] Additionally, the wavelength dependence of MOKE may be of rudimentary use for distinguishing the Kerr signal of different ferromagnetic elements in an alloy or a layered structure.

The physical origin of Q lies in the microscopic quantum behavior of electron-photon interactions in a magnetic solid. It is not possible to discuss this subject in any detail here; however, a few general comments can be made. Many early attempts to explain MOKE[6] used classical concepts and incorrectly attributed MOKE to a Lorentz type force caused by interactions between a ferromagnet's internal field and the electrons in the solid, which are also in the presence of a photon field. It is now generally agreed that the Kerr effect is a consequence of coupling between the spin of the moving electron in the solid and its momentum due to the net atomic potentials of the medium, i.e., spin–orbit coupling, a purely quantum
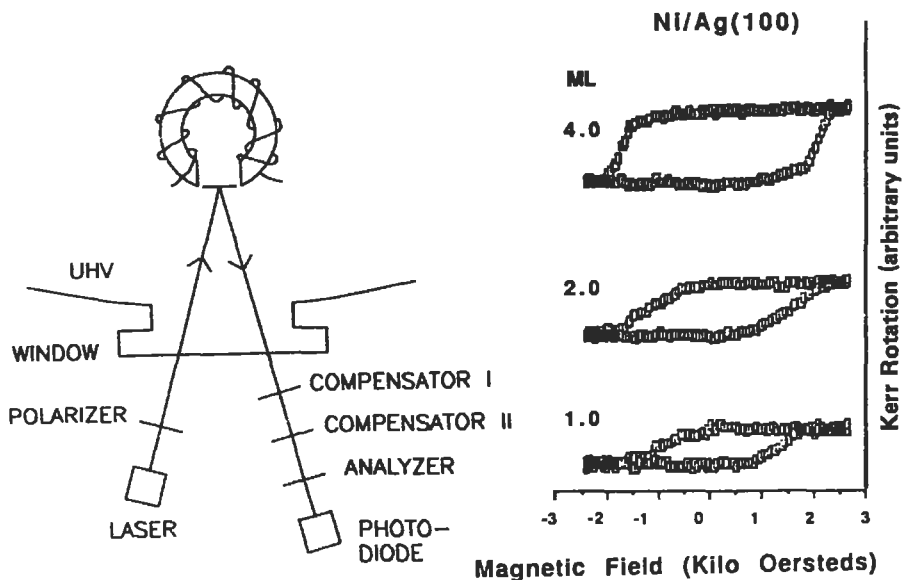
Figure 4 Schematic of an ultrahigh-vacuum MOKE experiment using the longitudinal geometry (a). An electromagnet is used to magnetize the sample in vacuum. The polarized light from a laser source shines through a window onto the sample; the reflected light passes through the window, a compensator (not required when only θ_K is measured), and an analyzing polarizer onto the photodiode detector.[11] Experimental hysteresis loops (b) for different thicknesses, in monolayers (ML), of Ni on Ag (100) taken by MOKE using a similar apparatus to (a), with the sample at 110 K.[3]

mechanical interaction. One consequence of the spin–orbit coupling is that the Kerr activity will be relatively large for materials with a large magnetic moment and with high atomic number. The first complete microscopic quantum theory of this effect was worked out by Argyres in 1955.[10] Nevertheless, it is still quite difficult, even today, to calculate the value of Q from first principles. Thus, absolute values of magnetization can, in general, be derived from MOKE only through careful calibration of appropriate known standards. Such calibrations require considerable care and often are unreliable, since the thickness and dielectric properties of the substrate, nonmagnetic overlayers, or windows in the optical path can have a considerable effect on the measured Kerr rotation in a real experiment.

Instrumentation

The instrumentation required to measure the hysteresis loop of a ferromagnetic surface with MOKE can be very simple. Figure 4a shows one such implementation of the experimental setup for analysis of ultrathin film samples maintained in a

ultrahigh-vacuum environment.[11] The Kerr rotation θ_K and the ellipticity ε_K can be determined from a dc measurement in this setup, although ac detection schemes are straightforward to implement using polarization modulation. Often an even simpler setup is used that does not include one, or either, of the compensators. In this case, a single rotation angle is measured that is directly related to θ_K but which is modified by any ellipticity introduced by the vacuum window. Figure 4b is an example of hysteresis loops measured for Ni films of 1–4 atomic layers using this general type of apparatus.[3a] The acceptable S/N shown here for this extreme thin-film limit demonstrates the broad applicability of MOKE. Many variations of this simple setup are discussed in the literature.[3] Additional cautionary notes are warranted here. Some of the components of the setup, especially the vacuum windows, may distort slightly as a function of the external H field and cause artifacts in the M–H loops by adding undetermined ellipticity to the true MOKE signal. Another problem may arise if vacuum containment windows are included in the experimental light path (see Figure 4, for example) when changes in the sample temperature are required, e.g., when measuring the temperature dependence of M. While MOKE has no inherent temperature dependence, small distortions of the sample or the experimental apparatus during heating and cooling may change the light path. Vacuum windows often are under nonuniform states of stress and very slight changes in the light path can result in spurious rotations and ellipticity changes of the light that are comparable to the Kerr response. Clearly, when $M(T)$ is to be measured by MOKE, such polarization changes must be avoided or compensated. Temperature dependent MOKE data have been reported where critical parameters of the magnetic state in ultrathin films were derived from the resulting, measured $M(T)$.[3, 12]

Imaging magnetic domains with MOKE or any other optical or electron imaging technique requires substantial magnification, since domains in interesting samples are typically small, on the order of 1–100 μm. Therefore, the instrumentation for Kerr microscopy requires the incorporation of basic polarization detection components with a high-quality optical microscope. In addition, much of the interest in imaging domains is in examining their dynamic behavior. This requires the addition of fast electronics capable of making MOKE measurements from ferromagnetic films switching at frequencies surpassing 1 MHz.[4] Figure 5 is an example of one such setup to image the dynamics of magnetic domains of magnetic recording heads using MOKE.[4b] Such microscopes generate a magnetization map of the head by spatially measuring the Kerr rotation in a point-by-point scan in steps of ~1 μm. Typically, the sample is moved under the polarized light, which is focused to about a 0.5-μm spot. Both the polar and longitudinal geometries are used in this setup. One useful kind of image obtained with this type of microscope shows just the changes in magnetization during a complete cycling of the head. (See Figure 6) The bright zones show the regions of the largest change in M, i.e., where the domain walls moved during a complete magnetization cycle. A variation on the
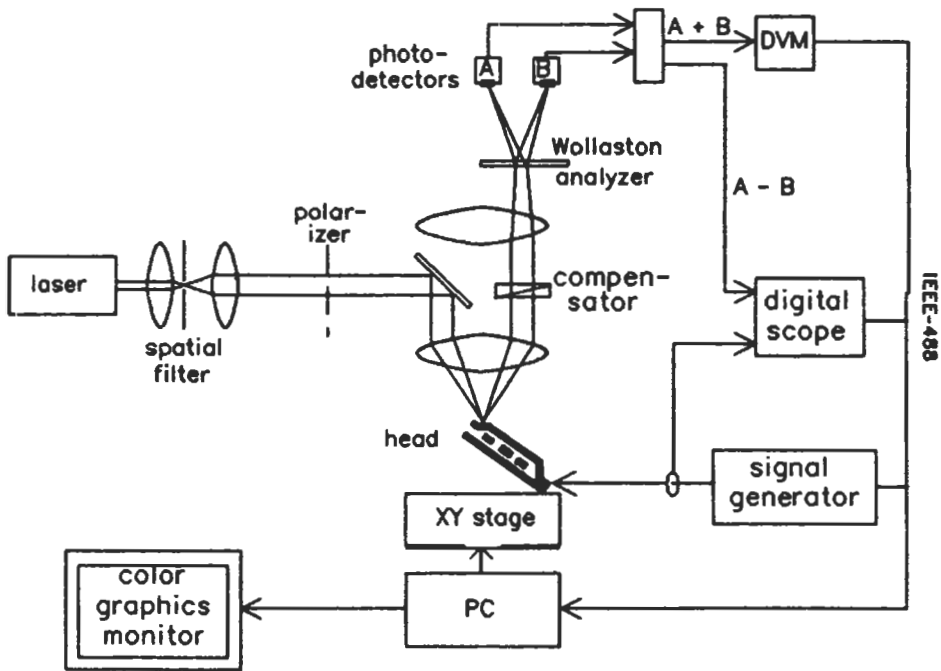
Figure 5   Schematic diagram of a Kerr microscopy apparatus.[4]

apparatus shown in Figure 5 provides a "parallel" method of generating the domain image.[13] A pulsed light source is defocused to illuminate a wide field of view in the microscope and the reflected light is collected by a time-synchronized video camera. A digital image for each time interval of interest can be stored and processed. The principle difference between the data provided by this approach and that of Figure 5 is that the former gives a domain image of a state of magnetization on a point-by-point basis, which is the average of many magnetization cycles, whereas the latter gives the instantaneous picture at all points in the field of view, at the resolution of the video digitizer, for a magnetization state from a single cycle. In the wide-field case the ratio S/N will be lower for a given spatial resolution. In either case, Kerr microscopy can be done using samples, with or without, thick transparent overlayers.

An interesting variation of the scanned sample, point-by-point experimental setup is the technological application of magneto-optic recording. A magneto-optic disk system is basically a miniaturized Kerr microscope using only the polar geometry. The magnetic sample or disk is rotated under the microscope, which moves radially from one track of magnetic domains or data bits to the next.
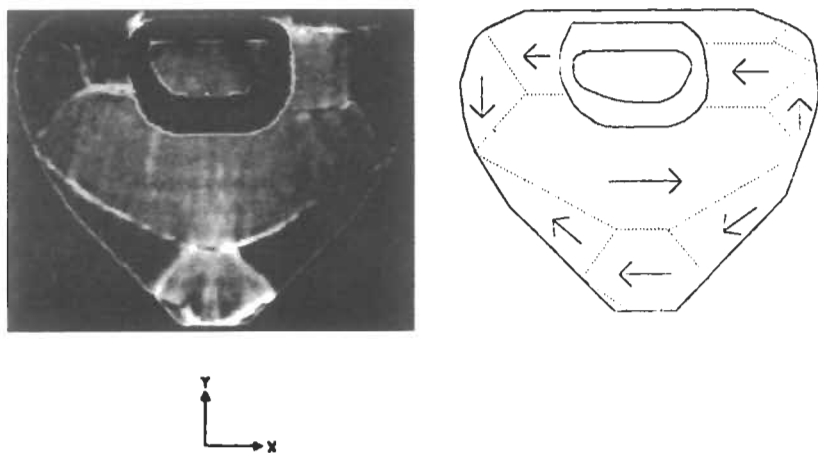
Figure 6   Scanning Kerr image of the magnetization changes in the *y*-direction for a thin-film head having a 1-MHz, 5-mA p–p coil current, and the magnetic domain pattern deduced for this head from the observed domain wall motion.[4a]

Comparison With Other Techniques

Even though MOKE is quite useful, it is not a panacea for all surface and interface magnetic characterization problems. It works best as a qualitative, diagnostic tool, as there is considerable difficulty in relating the Kerr rotation to the absolute value of M. This is the result of the complex coupling between the electronic band structure of the ferromagnet and incident light. Many other methods of characterizing ferromagnetic surfaces and interfaces exist, of course, and their use depends on which magnetic property, e.g., magnetization magnitude and orientation, magnetic anisotropy, or spin-dependent electronic band structure, is to be determined. Ferromagnetic resonance, FMR, is a technique that measures a quantity related to M and the anisotropy of the material. It is really a bulk technique, but can be applied to surfaces and interfaces in cases where these dominate the sample, as in ultrathin films and superlattices. Neutron reflectivity techniques, using polarized neutrons, are sensitive to the magnetization of a ferromagnet. These methods are rather specialized in view of the need for a neutron source, but they have the distinct advantage of being able to provide depth profiles of the magnetic moment. A large number of the standard electron spectroscopic techniques, including AES, UPS, LEED, and secondary electron emission, give signals related to the magnetic moment of a sample, when electron spin analysis is incorporated in the experiment. Any detailed comparison with these electron techniques is beyond our scope, but

because of their widespread use it is worth noting some practical differences relative to MOKE analysis:

1 They all require substantially more sophisticated apparatus to make a measurement.

2 The application of external magnetic fields to the sample during analysis presents considerable problems and constraints for electron techniques, whereas external fields have no influence on MOKE.

3 Most electron probes have more elemental specificity.

Operationally, the electron techniques all require high-vacuum or, more likely, ultrahigh-vacuum environments, and the magnetic material of interest must be within a few atomic layers of the surface. MOKE analysis is not restricted by these constraints, although interesting samples may be.

Kerr microscopy is an excellent method for making magnetic domain images and maps. Other useful techniques include the Bitter colloid technique, secondary electron microscopy with polarization analysis (SEMPA), microscopy using other electron emission spectroscopies (like AES) and Lorentz transmission electron microscopy (LTEM). The Bitter method is simple to use, but compared to MOKE, it suffers in that it contaminates the sample's surface, it cannot be used in the presence of external fields and its intrinsic response time limits its ability to follow the dynamics of domain motion to very low frequencies. SEMPA and LTEM have all the advantages and disadvantages of the other spin-resolved electron techniques discussed. With regard to imaging, SEMPA can be used at a much higher magnification and lateral resolution (~50 nm) than MOKE, but cannot follow domain wall motion at relevant frequencies due to S/N considerations. LTEM currently has the highest magnetic spatial resolution available, when used in the differential phase contrast mode. One significant drawback to LTEM analysis is the special and tedious requirement that the entire sample to be analyzed be thin enough (0.1–0.3 μm) to transmit the high-energy incident electrons in TEM. Further details regarding SEM and TEM analysis are given elsewhere in this volume. None of the other magnetic domain imaging techniques has the inherent speed of MOKE microscopy, which obtains useful imaging signals from thin films at frequencies in the MHz range. Thus, it is really the only imaging technique with the requisite spatial resolution to examine the switching of high-speed recording heads used in the magnetic recording industry.

Conclusions

MOKE measurements can be made using relatively simple and inexpensive apparatus, compared to most other surface magnetic probes and surface analytical techniques. MOKE is useful for the magnetic characterization of films of one to several monolayers, thin films, or the near-surface regions of bulk materials. MOKE has

been used most as a qualitative diagnostic of magnetic domain structure and domain dynamics. High spatial resolution can be obtained in this mode. Considerably less success has been achieved when attempting to make quantitative determinations of magnetic moment, with MOKE, because of the rather complex relationship of the Kerr rotation and ellipticity to the microscopic properties of the material, e.g., the magnetic moment and the electronic band structure.

MOKE will find continued application in analyses to determine the dynamics of domain motion in thin films and to determine values of the coercivity and information about magnetic anisotropies from hysteresis loop measurements. In addition, as the experimental method improves, reliable temperature-dependent MOKE measurements may become commonplace. There is considerable evidence that tuning the wavelength of the incident light to the dielectric properties of the magnetic film–substrate combination will offer somewhat enhanced Kerr rotations in the case of ultrathin films. As more wavelength-dependent studies are done and our knowledge of the detailed electronic band structure of alloys improves, one can expect progress in quantitative determinations of the magnetic moment of magnetic films and surfaces by MOKE. Nevertheless, a realistic assessment of MOKE in comparison with the spin-polarized electron spectroscopies suggests that the goal of obtaining moments at surfaces is more attainable using the electron spectroscopies. There is some potential for completely new methods and apparatus being developed in the field of MOKE analysis. For example, recent predictions[14] give rise to the possibility of developing intrinsically surface sensitive MOKE through the use of second harmonic detection of the reflected light. In such an experiment the intensity of the second harmonic light is quite low, but this light is emitted only from the surface or interfaces of the sample.

Related Articles in the Encyclopedia

SEM, TEM and VASE

References

1 K. Egashira and T. Yamada. *J. Appl. Phys.* **45**, 3643, 1974.

2 T. Katayama, Y. Suzuki, H. Awano, Y. Nishihara, and N. Koshizuka. *Phys. Rev. Lett.* **60**, 1426, 1988. A good demonstration of how the substrate influences MOKE in ultrathin films.

3 C. A. Ballentine, R. L. Fink, J. Araya-Pochet, and J. L. Erskine. *Appl. Phys. A.* **49**, 459, 1989; S. D. Bader, E. R. Moog, and P. Grünberg. *J. Magn. Magn. Mat.* **53**, L295, 1986.

4 P. Kasiraj, R. M. Shelby, J. S. Best, and D. E. Horne. *IEEE Trans. Mag.* **MAG-22,** 837, 1986; P. Kasiraj, D. E. Horne, and J. S. Best. *IEEE Trans. Mag.* **MAG-23,** 2161, 1987.

5 W. Reim. *J. Magn. Magn. Mat.* **58,** 1, 1986.

6 A. V. Sokolov. *Optical Properties of Metals.* Elsevier, New York, 1967, Chapters 10 and 11. A very detailed, mathematical description of solutions to the wave equations, with a nice historical perspective.

7 B. Thiel and H. Hoffmann. *J. Magn. Magn. Mat.* **6,** 309, 1977; C. C. Robinson. *J. Opt. Soc. Am.* **53,** 681, 1963. Dependence of MOKE on incidence angle.

8 P. Lorrain and D. Corson. *Electromagnetic Fields and Waves.* W. H. Freeman, San Francisco, 1970, p. 518. A general and clear text on electromagnetic wave phenomena at the undergraduate level.

9 T. E. Feuchtwang, P. H. Cutler, and J. Schmit. *Surf. Sci.* **75,** 401, 1978.

10 P. N. Argyres. *Phys. Rev.* **97,** 334, 1955. An excellent discussion of the quantum theoretical basis of MOKE.

11 E. R. Moog, C. Liu, S. D. Bader, and J. Zak. *Phys. Rev. B.* **39,** 6949, 1989.

12 C. Liu and S. D. Bader. in *Magnetic Properties of Low-Dimensional Systems* (L. M. Falicov, F. Mejia-Lira, and J. L. Moran-Lopez, eds.) Springer-Verlag, Berlin, 1990, vol. 2, p. 22.

13 D. A. Herman and B. E. Argyle. *IEEE Trans. Mag.* **MAG-22,** 772, 1986.

14 W. Hübner and K.-H. Bennemann. *Phys. Rev. B.* **40,** 5973, 1989.

12.4 Physical and Chemical Adsorption

Measurement of Solid Surface Areas

DAVID J. C. YATES

Contents

- Introduction
- Surface Areas by the BET Method
- Chemisorption
- Conclusions

Introduction

When a gas comes in contact with a solid surface, under suitable conditions of temperature and pressure, the concentration of the gas (the adsorbate) is always found to be greater near the surface (the adsorbent) than in the bulk of the gas phase. This process is known as *adsorption*. In all solids, the surface atoms are influenced by unbalanced attractive forces normal to the surface plane; adsorption of gas molecules at the interface partially restores the balance of forces. Adsorption is spontaneous and is accompanied by a decrease in the free energy of the system. In the gas phase the adsorbate has three degrees of freedom; in the adsorbed phase it has only two. This decrease in entropy means that the adsorption process is always exothermic. Adsorption may be either physical or chemical in nature. In the former, the process is dominated by molecular interaction forces, e.g., van der Waals and dispersion forces.[1] The formation of the physically adsorbed layer is analogous to the condensation of a vapor into a liquid; in fact, the heat of adsorption for this process is similar to that of liquefaction.

Chemical adsorption (known as *chemisorption*) often, but not invariably, involves the formation of a chemical bond (i.e., the transfer of electrons) between the gas and the solid. In other words, a specific chemical compound one layer thick
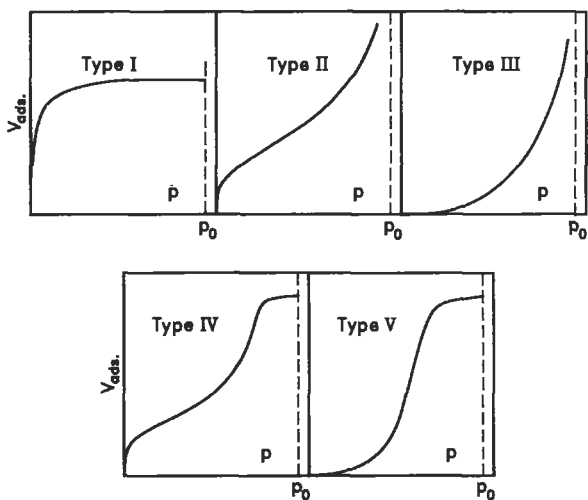
Figure 1 The five types of physical adsorption isotherms.[3]

(a *monolayer*) is formed between the adsorbate and the outer layer of the solid adsorbent The differences between physical and chemical adsorption have been discussed in detail,[1] but briefly they are as follows. Physically adsorbed gases can be removed readily from the adsorbent by evacuation at the same temperature at which adsorption took place. Chemisorbed gases can be removed isothermally in vacuum only rarely, especially on metal surfaces, where heating well above the adsorption temperature is usually required for complete desorption.

In this article, we will discuss the use of physical adsorption to determine the total surface areas of finely divided powders or solids, e.g., clay, carbon black, silica, inorganic pigments, polymers, alumina, and so forth. The use of chemisorption is confined to the measurements of metal surface areas of finely divided metals, such as powders, evaporated metal films, and those found in supported metal catalysts.

Surface Areas by the Brunauer, Emmett and Teller BET Method

The basic measurement of adsorption is the amount adsorbed v, which usually is given in units of cm^3 of gas adsorbed per gram of adsorbent. Usually this quantity is measured at constant temperature as a function of pressure p (in mm Hg), and hence is termed an isotherm. Isobars and isosteres also can be measured, but have little practical utility.[1] It has been found that isotherms of many types exist, but the five basic isotherm shapes are shown in Figure 1, where p_0 is the vapor pressure.

Type I isotherms occur only in systems where adsorption does not proceed beyond about one monolayer, and are found only in porous materials where the pore size is of molecular dimensions (e.g., zeolites and some carbons). Types IV and V are characteristic of multilayer adsorption on highly porous adsorbents, the flattening of isotherms near the saturation vapor pressure being due to the filling of capillaries. Type II isotherms are observed very commonly, being essentially the same as type IV isotherms except for the lack of capillary filling. Type III isotherms are but rarely found; they are usually a sign of a nonwetting system (e.g., the adsorption of water on a hydrophobic substance like pure charcoal). We will restrict our discussion in this article to types II and IV, as these isotherms are the only ones where the BET equation is applicable.

From an experimental point of view, the first step in determining an adsorption isotherm is to outgas the adsorbent. In the case of physical adsorption, this step serves to remove adsorbed water, and possibly other adsorbed gases, from the surface. This cannot be done efficiently by evacuation at room temperature, and is usually accelerated by heating the adsorbent. However, care must be taken to insure that the temperature maintained during the outgassing is not such[1] as to sinter the solid, and so decrease its surface area. In fact, it is only very recently that standardized methods for adsorption have been approved by the American Society for Testing and Materials (ASTM) Committee on Catalysts. In the formulation of the surface area standard,[2] the choice of degassing temperature occupied a considerable time, as no standard, or even recommendation for this temperature could be found in the earlier literature.[1] (This point, together with a detailed procedure for multipoint nitrogen isotherm determination for surface area by the BET method,[3] are discussed in the ASTM standard.) After outgassing, the next step is to determine the *dead space*. This is done by admitting a nonadsorbing gas, usually helium, when the cell is at the temperature at which the isotherm is to be measured. The initial pressure of the helium is measured by the pressure gauge in a system of accurately known volume. If a mercury manometer is used, the measuring side of the manometer must be kept at a fixed point in space when measuring the pressures. The author has found a commercially available quartz Bourdon gauge (of constant volume) to be much superior to any liquid manometer; the quartz gauge also has the advantage of keeping the system free of mercury or oil vapors. For example, a typical gauge I used[4] measured pressure changes as small as 0.004 cm, which is much better than can be realized with mercury manometers. In other words, helium at a known pressure and volume is admitted to the sample cell. From the pressure drop, the *effective* volume of the cell is determined. This procedure should be repeated several times. After this, the helium is evacuated, the cell shut and N_2 is admitted to the calibrated gauge volume. The gas pressure is measured, and the N_2 is admitted to the sample, which is held at 77 K. After allowing the pressure to come to equilibrium (which may take up to one hour) the final pressure is recorded. The same procedure is followed for the second and subsequent doses. The amount adsorbed is
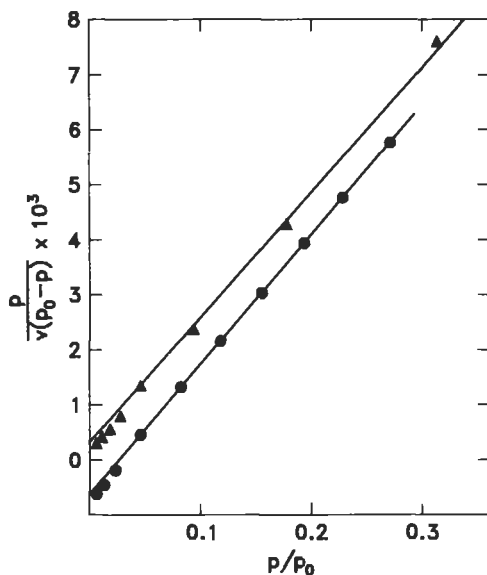
Figure 2   BET plots for N_2 at 90 K (filled circles) and > 77 K (filled triangles) on porous glass.[5]

calculated from the decrease in pressure beyond that expected from the increase in volume when the gas is admitted to the sample cell. Details of this procedure are given elsewhere.[2] Using the BET equation:

$$\frac{p}{v(p_0 - p)} = \frac{1}{v_m} + \left(\frac{c-1}{v_m c}\right)\frac{p}{p_0}$$

one plots $p/v(p_0-p)$ against p/p_0, as shown in Figure 2 for the adsorption of nitrogen at 77 K and 90 K on porous glass.[5]

In the BET equation, v is the volume of gas adsorbed in cm^3 at STP, per gram of solid at a pressure p. The constant c is related to the heat of adsorption[3] and v_m is the monolayer volume. From the plot one finds the slope $(1/v_m)$ and the intercept $1/cv_m$, so one can calculate v_m and c. At 90 K, v_m for the glass was 41.3 cm^3/gm, and assuming that nitrogen has a molecular area σ of 16.2 $Å^2$, one obtains[5] a surface area Σ of 179 m^2/gm. This value is obtained by using the equation $\Sigma = 0.269\ \sigma v_m$, where σ is in $Å^2$, v_m is in cm^3/gm, Σ is in m^2/gm, and the numerical factor comes from Loschmidt's number (molecules per cm^3 at STP). The values of σ usually are derived from the density of the liquid, and 16.2 $Å^2$ is the accepted value for nitrogen.[1,2] Values for other gases are given in Young and Crowell,[1] and this parameter is a critical one in determining surface area from the monolayer capacity. Finally, it should be noted that when isotherms are measured close to the boiling point of the adsorbed gas, e.g., for nitrogen adsorbed at 77 K, the range of

validity of the BET equation is in the relative pressure (p/p_0) range between 0.05 and 0.35, so that there is little point in measuring isotherms beyond those limits. In general, for best accuracy, at least four points should be measured in this region. Several other methods have been proposed for measuring surface areas by gas adsorption, (for example, the so-called *single-point* BET, in which the intercept value is ignored) and also by flow techniques (e.g., adsorption of N_2 from N_2:He mixtures) using a gas chromatography method, but an extensive review of these methods by the ASTM Committee on catalysts concluded that none were reliable, or as accurate, as the multipoint BET method, determined volumetrically.

While gravimetric methods that measure adsorption directly, for example, using helical quartz springs,[1] have been used in the past, the sensitivity in mass change per gram of adsorbent of early devices was very poor, and they were notoriously fragile and difficult to use. However, modern beam balances (e.g., the Cahn microbalance) have a much higher sensitivity, and their use has given accurate isotherms for ethylene adsorbed on a zeolite.[4] It also has been shown that the volumetric and gravimetric isotherms were in excellent agreement. This technique, however, is clearly more accurate for adsorbates of higher molecular weight; for instance, it has been rarely used to study the adsorption of hydrogen in chemisorption.

Chemisorption

This is a process that takes place via specific chemical forces, and the process is unique to the adsorbent or adsorbate used. In general, it is studied at temperatures much higher than those of the boiling point of the adsorbate; consequently, if supported metals are studied, little or no physical adsorption of the chemisorbing gas takes place on the high surface area support.

In particular, emphasis will be placed on the use of chemisorption to measure the metal dispersion, metal area, or particle size of catalytically active metals supported on nonreducible oxides such as the refractory oxides, silica, alumina, silica-alumina, and zeolites. In contrast to physical adsorption, there are no complete books devoted to this aspect of catalyst characterization; however, there is a chapter in Anderson[6] that discusses the subject.

As this field is very wide, we will discuss first the gases that can be used to study metal dispersion by selective chemisorption, and then some specific examples of their application. The choice of gases, is, of course, restricted to those that will strongly chemisorb on the metal, but will not physically adsorb on the support. Prior to determining the chemisorption isotherm, the metal must be reduced in flowing hydrogen; details are given elsewhere.[2] The isotherm measurement is identical to that used in physical adsorption.

The gases that have been used most often are hydrogen, carbon monoxide, and oxygen. Hydrogen is by far the most useful, and it has the best established adsorption mechanism. It dissociates at room temperature on most clean metal surfaces of
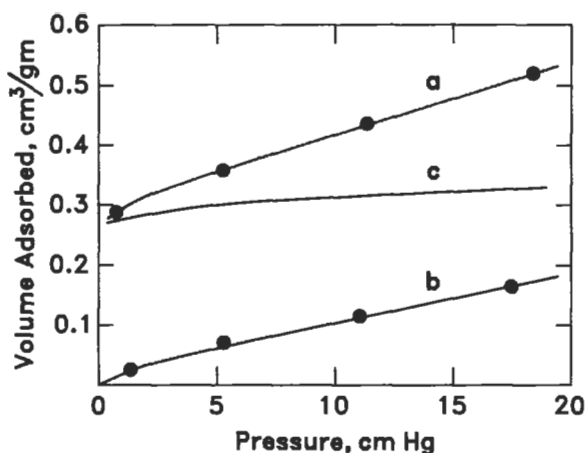
Figure 3 Adsorption isotherms[7] at room temperature on 0.1% Rh on silica: (a) CO isotherm; (b) CO isotherm after pumping out sample at end of isotherm (a) for 1 min; (c) difference between (a) and (b).

practical interest, one hydrogen atom being adsorbed per surface metal atom at saturation exposure. Due to its very low boiling point (20 K) there is no physical adsorption at room temperature on any support. Hydrogen can be used for all metals, with the exception of Pd, which forms bulk hydrides. If one knows the area occupied by one metal atom on the surface (readily obtained from crystallographic data) one can easily calculate the metal surface area from the monolayer capacity (v_m) of the adsorbed H_2.

The use of CO is complicated by the fact that two forms of adsorption—linear and bridged—have been shown by infrared (IR) spectroscopy to occur on most metal surfaces. For both forms, the molecule usually remains intact (i.e., no dissociation occurs). In the linear form the carbon end is attached to one metal atom, while in the bridged form it is attached to two metal atoms. Hence, if independent IR studies on an identical catalyst, identically reduced, show that *all* of the CO is either in the linear or the bridged form, then the measurement of CO isotherms can be used to determine metal dispersions. A metal for which CO cannot be used is nickel, due to the rapid formation of nickel carbonyl on clean nickel surfaces. Although CO has a relatively low boiling point, at very low metal concentrations (e.g., 0.1% Rh) the amount of CO adsorbed on the support can be as much as 25% of that on the metal; a procedure has been developed to accurately correct for this.[7] Also, CO dissociates on some metal surfaces (e.g., W and Mo), on which the method cannot be used.

Although considerable study has been devoted to oxygen chemisorption (mainly on platinum) there is considerable ambiguity in the surface stoichiometry of the reaction. In some cases Pt_2O is formed, in others PtO, the particular compound

being a function of different lattice planes exposed.[8] Hence, even for a noble metal like Pt, O_2 chemisorption is unreliable as a means of measuring metal surface area.[8] It also follows that other, more complicated methods, e.g., those involving the titration of adsorbed O_2 with H_2 are unreliable, and should not be used.

In contrast to such procedures as the use of the BET equation, there are no general procedures that can be specified as standards for chemisorption. For example, ASTM has published a detailed, standard method specifically for measuring H_2 chemisorption for platinum on alumina catalysts.[2] Not only is this restricted to one metal, but also to one support. In other words, there are specific features of the Pt on Al_2O_3 system which may well not be the same for the Pt on SiO_2 system. In addition, it is well known that other noble metals on Al_2O_3 behave very differently from Pt. As an example, in the standard test method, before the reduction of the catalyst it is advised that the catalyst be calcined in air. This is done by flowing air (using a special flow through adsorption cell, see Figure 2 of *Standard Test Method for Hydrogen Chemisorption on Supported Platinum on Alumina Catalysts*[2]) over the catalyst, then heating to 450° C, and holding for 1 hr at this temperature. After evacuating the air at 425° C, the catalyst is cooled. Hydrogen is then passed through the cell, and the sample is heated again to 450° C. After a hold period, the hydrogen flow is stopped, and the cell evacuated at 425° C. After cooling again, the chemisorption of H2 on the reduced catalyst is measured at room temperature. In the case of Pt on Al_2O_3 catalysts with Pt loading about 0.3%, the particle size of the platinum is very small, below 20 Å. In fact, one of the earliest[9] measurements of Pt dispersion on alumina, showed that nearly every Pt atom in the sample adsorbed one hydrogen atom, corresponding to a particle size of 10 Å. However, using the same support, alumina, but using 1% of iridium, the author has shown that a freshly prepared catalyst (air dried at 110° C) had an Ir particle size of 15 Å. If the procedure from *Standard Test Method for Surface Area of Catalysts* was followed (an *in situ* oxidation at 450° C), followed by a H_2 reduction at 450° C, then the Ir particle size was found to be 50 Å. In other words, air treatment of a platinum catalyst at 450° C has no deleterious effect on the metal dispersion, while drastically reducing the dispersion of iridium. Thus, following the "standard" procedure[2] for platinum would give entirely erroneous data for iridium. This is despite the general similarity of the two elements; it is due to the fact that after an oxidation treatment platinum remains as metallic particles, while the iridium forms 50A oxide particles on heating to 540° C,[10] as shown by X-ray diffraction.

To give an idea of the wide range of catalytic systems that have been investigated where chemisorption data were essential to interpret the results, some of the author's papers will be discussed. Measurements were reported on the surface areas of a very wide range of metals that catalyze the hydrogenation of ethane.[7, 11–14] In the earliest paper, on nickel, the specific catalytic activity of a supported metal was accurately measured for the first time; it was shown also that the reaction rate was directly proportional to the nickel surface area.[11] Studies on the same reaction

showed quite a marked variation in the nickel surface area when the support was changed—a factor of 2. However, a factor of 50 was found between the most active and least active catalyst, when expressed on a constant nickel surface area basis, due to effect of the support. Later work showed that the specific catalytic activity for 1% Ni on SiO_2 was about a hundredfold less than that of 10% Ni on the identical support. Using the most "inert" support, pure SiO_2, a series of metals were studied (Co, Pt, and Cu), all at 10% concentration and the specific catalytic activities of the metals were found to follow the order Ni > Co > Pt.[12] Other noble metals of known particle size were studied on the same silica,[12] and the order of activity was found to be Ru > Rh > Ir > Pd = Pt. For all group VIII metals the relative specific activity was not correlatable with any single property of the metal itself (e.g., % d character) but was dependent on both the % d character and the atomic radius.[13] The elements Ni and Co were on one line in the relation between the specific activity and % d character and the noble metals on another, very different, line (i.e., Ru, Rh, Pd, Ir and Pt).

Finally, the same reaction was studied with a series of unsupported Ni:Cu alloys.[14] In all cases, the total surface areas (equal to the metal area for an unsupported metal) of the pure catalysts and the eight alloys were measured by the BET method, using argon isotherms measured at 77 K. For all catalysts, hydrogen chemisorption was also measured. After the first H_2 isotherm, the catalysts were evacuated for 10 minutes, and H_2 readsorbed. The second isotherm measured the weakly adsorbed H_2. With pure copper, as expected, the total H_2 chemisorption was the same as the weakly adsorbed H_2; in other words, there was *no* strongly adsorbed H_2 on pure Cu. For pure Ni, in contrast, the weakly adsorbed H_2 was about 20% of the total H_2 adsorption. This technique enabled the *surface* composition of the alloys to be directly measured. It was shown for the first time that a catalyst containing 5% Cu overall had a surface composition in the range of 50% Cu. It should be noted here that although one can estimate the surface composition of such alloys by ESCA, Auger, or other spectroscopic techniques, they usually do not give selectively the composition of just the surface layer of metal atoms. The Auger electrons, for example, come from an escape depth equivalent to several atom layers. Auger spectroscopy is very difficult to use with insulating systems; it is less of a problem with ESCA. Some techniques do have very short probing depths, e.g., low-energy ion scattering spectroscopy (ISS), which gives essentially the top layer composition.

Conclusions

Both of the surface area techniques described in this article are well established. However, the determination of total surface area by physical adsorption using the BET equation is a very general method of wide applicability. The use of selective chemisorption to determine the surface area of metals is much newer, and has only

been systematically applied in the last 20 years or so. It is expected that more metals than those discussed will be studied in the future. As mentioned, the method of measuring the surface area of supported metals is by no means the same for all metals. For example, Pt and Ir catalysts have to be prepared, calcined, and reduced in very different fashions, depending on the chemistry of the particular metal. In other words, very much depends on the particular knowledge of the individual investigator in studying supported metals.

Related Articles in the Encyclopedia

None

References

1 D. M. Young and A. D. Crowell. *Physical Adsorption of Gases.* Butterworths, London, 1962.

2 *Standard Test Method for Surface Area of Catalysts.* (D3663–78); *Standard Test Method for Hydrogen Chemisorption on Supported Platinum on Alumina Catalysts.* (D3908–80) American Society for Testing and Materials (ASTM), Philadelphia, PA.

3 S. Brunauer, P. H. Emmett, and E. Teller. *J. Amer. Chem. Soc.* **60,** 309, 1938.

4 D. J. C. Yates. *J. Phys. Chem.* **70,** 3693, 1966.

5 D. J. C. Yates. *Proc. Roy. Soc.* **A224,** 526, 1954.

6 J. R. Anderson. *Structure of Metallic Catalysts.* Academic Press, London, 1975.

7 D. J. C. Yates and J. H. Sinfelt. *J. Catal.* **8,** 348, 1967.

8 G. R. Wilson and W. K. Hall. *J. Catal.* **17,** 190, 1970.

9 L. Spenadel and M. Boudart. *J. Phys. Chem.* **64,** 604, 1960.

10 D. J. C. Yates and W. S. Kmak. (1979) US patent no. 4,172,817.

11 D. J. C Yates, W. F. Taylor, and J. H. Sinfelt. *J. Amer. Chem. Soc.* **86,** 2996, 1964.

12 W. F. Taylor, D. J. C. Yates, and J. H. Sinfelt. *J. Phys. Chem.* **69,** 95, 1965.

13 J. H. Sinfelt and D. J. C. Yates. *J. Catal.* **8,** 82, 1967.

14 J. H. Sinfelt, J. L. Carter, and D. J. C. Yates. *J. Catal.* **24,** 283, 1972.